INVITED COMMENT

Projection techniques to approach the nuclear many-body problem

IOP Publishing | Royal Swedish Academy of Sciences Physica Scripta

Phys. Scr. **91** (2016) 043005 (23pp) doi:10.1088/0031-8949/91/4/043005

Invited Comment

Projection techniques to approach the nuclear many-body problem

Yang Sun

Department of Physics and Astronomy, Shanghai Jiao Tong University, Shanghai 200240, People's Republic of China
Collaborative Innovation Center of IFSA (CICIFSA), Shanghai Jiao Tong University, Shanghai 200240, People's Republic of China
State Key Laboratory of Theoretical Physics, Institute of Theoretical Physics, Chinese Academy of Sciences, Beijing 100190, People's Republic of China

E-mail: sunyang@sjtu.edu.cn

Received 27 November 2015, revised 31 January 2016
Accepted for publication 11 February 2016
Published 22 March 2016

Abstract

Our understanding of angular–momentum-projection goes beyond quantum-number restoration for symmetry-violated states. The angular–momentum-projection method can be viewed as an efficient way of truncating the shell-model space which is otherwise too large to handle. It defines a transformation from the intrinsic system, where dominant excitation modes in the low-energy region are identified with the concept of spontaneous symmetry breaking, to the laboratory frame with well-organized configuration states according to excitations. An energy-dictated, physically-guided shell-model truncation can then be carried out within the projected space and the Hamiltonian is thereby diagonalized in a compact basis. The present article reviews the theory of angular–momentum-projection applied in the nuclear many-body problem. Angular momentum projection emerges naturally if a deformed state is treated quantum-mechanically. To demonstrate how different physical problems in heavy, deformed nuclei can be efficiently described with different truncation schemes, we introduce the projected shell model and show examples of calculation in a basis with axial symmetry, a basis with triaxiality, and a basis with both quasiparticle and phonon excitations. Technical details of how to calculate the projected matrix elements and how to build a workable model with the projection techniques are given in the appendix.

Keywords: shell model, angular momentum projection, deformed basis

1. Introduction

The nuclear shell model, for which we refer to the conventional shell model based on the spherical basis, is thought to be the most fundamental way of describing many-nucleon systems [1]. To compare with many other nuclear many-body techniques [2] a shell-model calculation is conceptually simple and straightforward: one builds a many-body configuration basis, chooses a reasonable Hamiltonian for that basis, and then performs a numerical diagonalization. Once a calculation is done, one expects to get, at least in principle, all types of low-energy excitations. In practice, however, using such a shell model to study arbitrarily heavy, deformed nuclei is impossible because of the huge dimensionality of the configuration space and related problems. Even with today's computer power, standard shell-model diagonalizations are usually done up to the mass-70 region, for which dimension of the configuration space may reach one billion. For heavy mass regions, a general application of the spherical shell model is out of question and one can only perform selected calculations for nuclei lying not far from the closed shells.

To study heavy, deformed nuclei where collective motion is the dominant excitation mode in the low-energy region [3], one relies mainly on the mean-field approximations, in which

the concept of spontaneous symmetry breaking is applied [2, 4, 5]. The mean-field approximations, such as the Hartree–Fock, the BCS, or the Hartree–Bogolyubov method, usually violate the invariance of the system. In particular, a deformed basis is associated with breaking of rotational symmetry and angular momentum in a deformed basis is no longer a conserved quantum number. Although in many circumstances interesting physics can be discussed in deformed bases attached to the system (the intrinsic frame) [5], the broken rotational symmetry should, in principle, be restored if the system in question is not of a macroscopic size. One common method to restore the breaking rotational symmetry is through angular–momentum-projection [2], which corresponds to a transformation from the intrinsic frame to the laboratory frame where observables are defined.

There are two different kinds of basic philosophy as far as the angular–momentum-projection is concerned. The first one aims mainly to restore the angular-momentum quantum number violated in the deformed mean-filed wave function and discuss the related effects. For example, exact (three-dimensional) angular–momentum-projection from the cranked Hartree–Fock-Bogoliubov (HFB) wave functions in heavy nuclei was performed [6, 7] to investigate the validity of the Kamlah expansion [8] which has been widely used in the literature for approximate projection. Angular–momentum-projection together with particle-number-projection calculation was carried out [9, 10] for the cranked HFB self-consistent solution to overcome the difficulty of a mean field theory in the calculation of electromagnetic transition rates. It was suggested [10] that the construction of exact eigenstates of angular momentum paves a way for the calculation of interband and intraband electromagnetic transition rates, which is not possible for wave functions that are not eigenstates of angular momentum. In another example, angular–momentum-projection was applied to calculate $B(E3)$ transition probabilities of spherical or soft nuclei with the density-dependent Gogny force [11, 12]. Much enhanced transition probabilities were obtained as compared to the unprojected results with a rotational-model assumption [11], indicating a gain of correlation. Thus it is important to emphasize that, while the violated quantum number is restored, additional correlations are gained through angular–momentum-projection. Therefore, one usually refers the method to beyond-mean-field.

Considerable progress has recently been made to combine the projection calculation with generator coordinate method (GCM) to describe shape variations and low-lying collective excitations (see, for example [13]). These beyond-mean-filed methods, which represent the state-of-the-art many-body technique, start from very different (non-relativistic or relativistic) effective interactions but carry out similar symmetry restoration and configuration mixing process for their respective mean-filed solutions. The discussed physics has been concentrated on low-spin, low-excited states in doubly-even nuclei. As for instance, [14] used the Gogny D1S interaction and studied coexistence of multiple shapes in the $N = Z$ nucleus ^{80}Zr. Reference [15] started from a Skyrme energy density functional with the constrained results of axial deformation, and performed angular–momentum-projection and configuration mixing calculation for the neutron-deficient lead region where shape coexistence is well known. Only qualitative agreements with experimental data were achieved possibly due to the improper single-particle states generated by the Skyrme force [15]. In another example [16], neutron-deficient Krypton isotopes were studied by the beyond relativistic mean-filed method generated by the PC–PK1 force plus BCS model. Configuration mixing was performed for both particle-number and angular-momentum projected axially-deformed states in the content of GCM. Compared with those previously calculated results with the Gogny and the Skyrme forces, it was concluded [16] that the results obtained from different types of forces are similar.

The second basic philosophy with angular–momentum-projection is different. It views the angular–momentum-projection as an efficient way of truncating the shell model space which is otherwise too large to handle. From the view point of quantum mechanics, it does not matter how to prepare a model basis, it is however important in practice to use the most efficient one. If one considers the fact that except for a few lying in the vicinity of shell closures, most nuclei in the nuclear chart are deformed, one should recognize that using a spherical basis to describe deformed nuclei is not an optimal choice. A deformed basis with a deformation closer to the 'true' deformation of a nucleus should be more economic. Furthermore, a deformed basis incorporates efficiently important correlations through the concept of spontaneous symmetry breaking. The violated quantum numbers in the wave functions can be recovered by the projection technique. The shell-model diagonalization is then carried out in the projected basis defined in the laboratory frame. Thus regarding shell-model calculations for arbitrarily heavy nuclei, working with deformed bases is a wise choice, and very likely the only choice, as far as the computation feasibility is concerned.

Moreover, feasibility in computation is not our only concern. To extract physics from the vast amount of computer output of a large-scale shell-model calculation [1] is generally difficult. It is thus very desirable to use an optimal basis, which has a classification scheme in the sense that a simple configuration corresponds approximately to a low excitation mode of the nucleus. Working in an optimal basis not only can simplify the calculation, but also make physical interpretation more easy and transparent. Even though an optimal basis is not used in the initial shell-model calculation, one transfers the shell-model results to it in order to discuss the physics [17, 18].

A deformed basis consists of an optimal set of basis states for a deformed nucleus. In the long history of the shell model, Elliott was the first to point out the advantage of a deformed (intrinsic) many-body basis and developed the SU(3) shell model [19] for sd-shell nuclei. In this model, the classification of basis states and their projection onto good angular momenta can be carried out using the group theoretical method. It works nicely so long as the spin–orbit force is weak (the L–S coupling scheme). In heavier nuclei, where the presence of a strong spin–orbit force (the j–j coupling

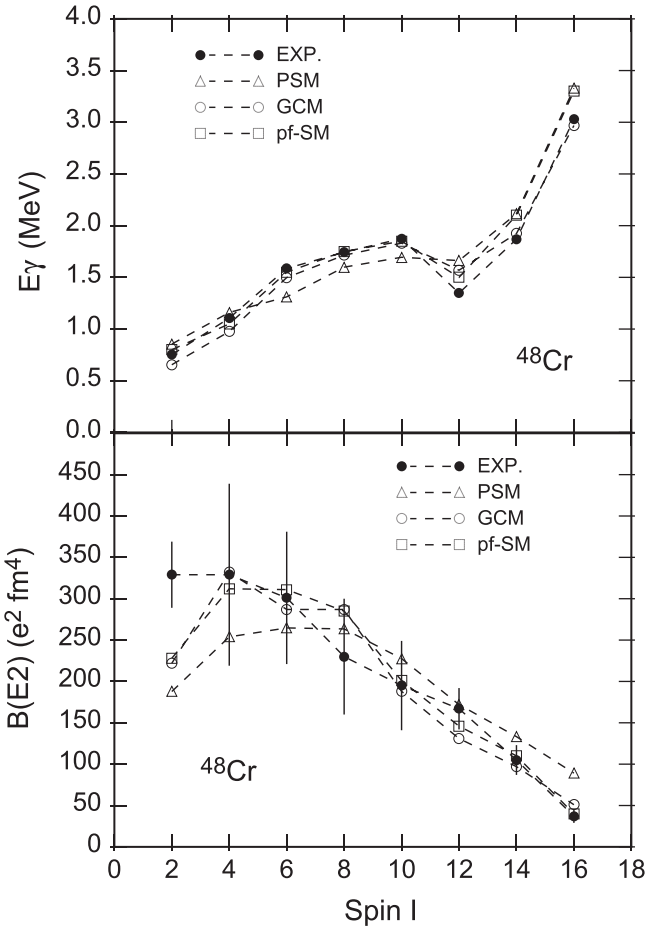

Figure 1. Top: γ-ray transition energies $E_\gamma = E(I) - E(I-2)$ as functions of spin. Bottom: B(E2) values as functions of spin. The experimental data are taken from [29], and the results of *pf*-SM from [30] and those from the PSM and GCM from [31]. This figure is reconstructed from figures 1 and 2 of [31] and reproduced with permission. Copyright APS 1991.

scheme) is essential for the correct shell closures (or magic numbers), the SU(3) scheme is no longer valid. For such systems, we may resort to the Nilsson model [20] (more precisely the Nilsson+BCS scheme if one takes the strong pairing correlations into account) and project numerically the deformed (multi-quasiparticle) basis onto good angular momenta (and particle number). In this way, we come to the basic idea of the projected shell model (PSM) [21] approach that has been proven successful in describing both low-lying and high-spin states of deformed nuclei. The PSM can be considered to be a natural extension of the Elliott SU(3) shell model to heavier systems, which makes shell-model calculation for heavy, deformed nuclei feasible [22–25]. Models based on the second philosophy were developed by the Tübingen group [26–28].

It has been well established that for a description of excitation modes including the collective rotations and quasiparticle (qp) excitations associated with a well-deformed energy minimum, the PSM introduces a very efficient truncation scheme. Diagonalization for a heavy nucleus can be done almost instantly with a personal computer, yet the results are often satisfactory. The reason for the success is because the major part of the essential correlations in nuclei has already been built in the basis through the use of a properly-chosen deformed basis. Therefore, a small qp configuration space built with only a few single-particle orbits around the Fermi surface can already span a very good basis for low-energy excitations. Note that each of the configurations in the PSM basis is a complex mixture of multi-shell configurations of the spherical shell-model space. Although the final dimension for diagonalization in the PSM approach is small, it is huge in terms of conventional shell-model configurations. We shall see an example next to show the efficiency of working with a deformed basis for shell-model calculations.

2. Spherical basis versus deformed basis

For a shell-model calculation, the results should in principle not depend on how the model basis is prepared. We take an example to show that a same description for energy levels and electromagnetic transitions can be achieved by using both spherical and deformed bases, as far as the yrast spectrum is concerned. ^{48}Cr is a nucleus for which a large-scale shell-model calculation based on a spherical basis can be done, yet exhibits remarkable high-spin phenomena usually observed in heavy nuclei, such as large deformation, rotational spectrum, and the backbending in moment of inertia in which the regular rotational band is suddenly disturbed at the angular-momenta $I = 10$–12 [29]. Caurier *et al* demonstrated [30] that the *pf*-shell model (*pf*-SM) can provide an exact solution of the Hamiltonian within the *pf*-shell, and their SM results for ^{48}Cr indeed reached an excellent agreement with the known experimental data [29].

However, in the *pf*-SM calculation in [30], or in spherical shell-model calculations in general, a single shell-model configuration does not correspond to any real excitation mode of a deformed nucleus such as ^{48}Cr, and therefore millions of many-body basis states are necessary even to represent the lowest eigenstate of the Hamiltonian. As a result, the physical insight is lost and interpretation of the result becomes difficult. In other words, in spherical shell-model calculations, angular momentum is conserved but the physical insight, associated with the existence of an optimal basis with the intrinsic states, can not be extracted. Therefore, in the same collaboration [30], cranked HFB calculations with the finite-range density-dependent Gogny force were also performed and the physics of ^{48}Cr was interpreted in the intrinsic frame, which however does not conserve angular momentum.

It is desirable to have a method that can combine advantages of the above two approaches, namely, the mean-filed theory and the (spherical) shell model. Such a method starts from a deformed solution obtained in the intrinsic basis similar as the HFB theory in [30], but transforms the basis states from the intrinsic to the laboratory frame through angular–momentum-projection, builds configurations in the projected space, and then carries out shell-model diagonalization in that new basis defined in the laboratory frame.

The latest step is the shell-model diagonalization as in [30]; the difference is that the size of the new, angular-momentum-projected basis is much smaller than the original *pf*-SM one. As we show below, the PSM approach provides such an example [31].

Before we discuss details of how an angular–momentum-projection calculation is carried out, let us compare the results obtained from three different model-calculations for ^{48}Cr. In the upper plot of figure 1, the PSM results along the yrast band of ^{48}Cr for the γ-ray transition energies, $E_\gamma = E(I) - E(I-2)$, together with those of the *pf*-SM in [30], are compared with the experimental data [29]. In figure 1, there is another set of results obtained by the GCM [32] with the same Hamiltonian as used in the *pf*-SM calculation [30]. One sees that the curves in the comparison are bunched together over the entire spin region, indicating an excellent agreement of the three theories with each other, and with the data. The sudden drop in E_γ occurring around spin $I = 10$ and 12 corresponds to the experimentally-observed backbending in the yrast band of ^{48}Cr.

In the lower plot of figure 1, the theoretical results for B(E2) are compared with the data [29]. All the three theories used the same effective charges (0.5e for neutrons and 1.5e for protons). Again, one sees that theories agree well not only with each other but also with the data. The B(E2) values decrease monotonously after spin $I = 6$. This implies a monotonous decrease of the intrinsic Q-moment as a function of spin, reaching finally the spherical regime at higher spins. This feature was explicitly discussed in [30] within the cranked HFB framework.

The above results indicate that the PSM, starting from a deformed intrinsic basis with angular–momentum-projection, is a reasonable shell-model truncation scheme as it reproduces the result of the *pf*-SM very well and describes the same physics about ^{48}Cr. Similarly, there has been another example for the superdeformed band of the lighter $N = Z$ nucleus ^{36}Ar [33, 34], for which the shell models based on spherical and deformed bases work equally well [35, 36].

There is of course one other question: how much the shell-model results depend on the interaction? The PSM results shown in figure 1 uses a schematic Hamiltonian [31] (see discussions in section 4) while the *pf*-SM the Hamiltonian based on the Kuo–Brown G matrix [37] known as the KB3 effective force [38]. The answer to the question how the PSM can obtain a similar result was discussed in [21]. It was shown that the rotational feature of the band energies does not depend on details of the Hamiltonian, and that any (rotation invariant) Hamiltonian, which delivers similar values for (1) the fluctuation of the angular momentum, (2) the Peierls–Yoccoz moment of inertia [2], and (3) the qp excitation energies, will lead essentially to the same result. Among the above three conditions, the first two are for the ground state properties that determine the scaling of band energies while the last one ensures the correct relative position of various bands reflecting the shell filling of the nucleus in question. Theories that treat angular momentum properly, either within the large-scale shell-models or with the angular–momentum-projection, will likely satisfy the first two conditions. To satisfy the last condition, one may introduce the monopole corrections [39] to the effective interaction to obtain correct single-particle states for large-scale SM calculations, or adopt well-established single-particle states that are empirically fitted to experimental data (such as those of the deformed Nilsson model [40]) as a starting basis.

The use of a deformed basis for shell model calculations can be traced back to the Elliott work [19], who was in the early days to recognize the advantage to describe rotational bands. Deformed mean field has been widely used in nuclear calculations [2]. The term 'shell model' is used mainly for the models based explicitly on diagonalization of (rotational-invariant) two-body interactions, sometimes referred to as 'spherical shell model'. Somewhat incorrectly, following the tradition of the early 1950s of the last century, the mean-field theory was referred to as 'deformed shell model' (typically in the context of the Nilsson model). On the other hand, the term 'beyond-mean-field', which largely takes the advantage of deformed basis, means 'projection methods in the context of the mean field approach'. These approaches usually use the energy density functional, not a two-body Hamiltonian, and therefore, do not belong to the shell model family.

Now let us discuss the theory of angular–momentum-projection and use it to approach the nuclear many-body problem.

3. Derivation of angular–momentum-projection

We first show that angular–momentum-projection emerges naturally if a deformed state is treated fully quantum-mechanically in the rotational space.

As the problem is related to rotation in space, we start the discussion with the rotation group whose elements are specified by the group parameter Ω, which represents a set of Euler angles (α, $\gamma = [0, 2\pi]$ and $\beta = [0, \pi]$). The explicit form of the group element is [41]

$$\hat{R}(\Omega) = \mathrm{e}^{-\imath\alpha\hat{J}_z}\mathrm{e}^{-\imath\beta\hat{J}_y}\mathrm{e}^{-\imath\gamma\hat{J}_z}, \tag{1}$$

where $\hat{J}_i$'s ($i = x, y, z$) are the angular momentum operators. Its (unitary) representation is

$$\langle \mu IM|\hat{R}(\Omega)|\nu JK\rangle = \delta_{\mu\nu}\delta_{IJ}D^{I*}_{MK}(\Omega) \tag{2}$$

where the symbol $*$ means the complex conjugation and $D^I_{MK}(\Omega)$ is the D-function [41]. The D-functions form a complete set of functions in the parameter space of Ω. For a state $|\mu IM\rangle$ belonging to the angular momentum IM, μ designates a set of quantum numbers that specify the quantum state uniquely, so that the following closure holds:

$$\sum_{\mu IM}|\mu IM\rangle\langle\mu IM| = 1. \tag{3}$$

We need not to know details of the state $|\mu IM\rangle$, except for the fact that it belongs to a complete set of orthonormal vectors in a Hilbert space in which the operator (1) acts. From

equations (2) and (3), it follows that

$$\hat{R}(\Omega)|\nu IK\rangle = \sum_{M}|\nu IM\rangle D^{I*}_{MK}(\Omega) \tag{4}$$

which is the multiplet relation between the states belonging to a representation (angular momentum) I.

Now let us suppose that $|\Phi\rangle$ is a deformed state that is not an eigenstate of angular momentum. $|\Phi\rangle$ may be obtained as a solution of the above mentioned mean-field calculations. For a rotationally-invariant Hamiltonian

$$\hat{R}^{\dagger}(\Omega)\hat{H}\ \hat{R}(\Omega) = \hat{H}, \tag{5}$$

the following identity for the energy expectation value holds

$$\frac{\langle\Phi|\hat{H}|\Phi\rangle}{\langle\Phi|\Phi\rangle} = \frac{\langle\Phi|\hat{R}^{\dagger}(\Omega)\hat{H}\hat{R}(\Omega)|\Phi\rangle}{\langle\Phi|\hat{R}^{\dagger}(\Omega)\hat{R}(\Omega)|\Phi\rangle}. \tag{6}$$

This means that the energy expectation value remains the same when the state $|\Phi\rangle$ is rotated in space. In other words, all rotated states, $\hat{R}(\Omega)|\Phi\rangle$, having different orientations Ω are mutually degenerate. As $\hat{R}(\Omega)|\Phi\rangle$ represents states with certain space orientation Ω, it is linearly independent of any other state with Ω'. Thus the general presentation is written by taking a superposition of all the rotated states

$$|\Psi\rangle = \int \mathrm{d}\Omega\, F(\Omega)\hat{R}(\Omega)|\Phi\rangle. \tag{7}$$

Peierls and Yoccoz proposed equation (7) as an ansatz of the wave function [42], which may be viewed a special case of the generator-coordinate wave function of Griffin, Hill, and Wheeler [43], with $F(\Omega)$ being the generator function. $F(\Omega)$ can in principle be determined by minimizing the energy expectation value

$$E = \frac{\langle\Psi|\hat{H}|\Psi\rangle}{\langle\Psi|\Psi\rangle}. \tag{8}$$

Solving for $F(\Omega)$ is generally a nontrivial task. However, for the present special case, one can greatly simplify the variational procedure by making use of the completeness of the D-functions. We can first expand the generator function $F(\Omega)$ as

$$F(\Omega) = \sum_{IMK}\frac{2I+1}{8\pi^2}F^{I}_{MK}D^{I}_{MK}(\Omega) \tag{9}$$

and then insert it into equation (7) to obtain

$$|\Psi\rangle = \sum_{IMK}F^{I}_{MK}\hat{P}^{I}_{MK}|\Phi\rangle. \tag{10}$$

The operator $\hat{P}^{I}_{MK}$ in equation (10) is defined as

$$\hat{P}^{I}_{MK} = \frac{2I+1}{8\pi^2}\int \mathrm{d}\Omega\, D^{I}_{MK}(\Omega)\hat{R}(\Omega), \tag{11}$$

which is called the angular–momentum-projection operator. $\hat{P}^{I}_{MK}|\Phi\rangle$ in (10) is thus the (angular–momentum) projected state. The coefficients F^{I}_{MK} in (10) play the role of the variational parameters in place of the generator function $F(\Omega)$ in (7). Now $|\Psi\rangle$ in (10) is expressed as a linear combination of a set of states created by the operator $\hat{P}^{I}_{MK}$ acting on the deformed state $|\Phi\rangle$.

Using equation (4) and the orthogonality of the D-functions [41]

$$\int \mathrm{d}\Omega\, D^{I*}_{MK}(\Omega)D^{I'}_{M'K'}(\Omega) = \frac{8\pi^2}{2I+1}\delta_{II'}\delta_{MM'}\delta_{KK'}, \tag{12}$$

one obtains the relation

$$\hat{P}^{I}_{MK}|\nu I'K'\rangle = \delta_{II'}\delta_{KK'}|\nu IM\rangle. \tag{13}$$

From equations (3) and (13), one can obtain its spectral representation and the 'sum rule'

$$\hat{P}^{I}_{MK} = \sum_{\nu}|\nu IM\rangle\langle\nu IK|, \quad \sum_{IM}\hat{P}^{I}_{MM} = 1. \tag{14}$$

Using the spectral representation, one can easily derive the properties for the angular–momentum-projection operator

$$\hat{P}^{I\,\dagger}_{MK} = \hat{P}^{I}_{KM} \text{ and } \hat{P}^{I}_{KM}\hat{P}^{I'}_{M'K'} = \delta_{II'}\delta_{MM'}\hat{P}^{I}_{KK'}. \tag{15}$$

If we carry out the variational procedure with the trial wavefunction of equation (10), it is easy to show that the summation over I and M actually drops away due to equations (5) and (15), and the state therefore has a sharp I and M. Thus, it is sufficient to carry out the variational calculation with

$$|\Psi\rangle = \sum_{K}F^{I}_{K}\hat{P}^{I}_{MK}|\Phi\rangle \tag{16}$$

without the summation over I and M. This means that $|\Psi\rangle$ becomes an eigenstate of angular momentum. The rotational symmetry violated in the deformed state $|\Phi\rangle$ is thus recovered in the new state $|\Psi\rangle$.

The resulting variational equation takes the form of the generate-coordinate equation of Griffin, Hill, and Wheeler [43], and is an eigenvalue equation with the normalization condition written in a nonorthogonal basis:

$$\sum_{K'}\{H^{I}_{KK'} - EN^{I}_{KK'}\}F^{I}_{K'} = 0, \tag{17a}$$

$$\sum_{KK'}F^{I}_{K}N^{I}_{KK'}F^{I}_{K'} = 1, \tag{17b}$$

in which the Hamiltonian matrix and norm matrix are defined as

$$H^{I}_{KK'} = \langle\Phi|\hat{H}\hat{P}^{I}_{KK'}|\Phi\rangle, \tag{18a}$$

$$N^{I}_{KK'} = \langle\Phi|\hat{P}^{I}_{KK'}|\Phi\rangle. \tag{18b}$$

Thus we have shown that solving the eigenvalue equations of (17) is equivalent of performing the variational calculation from which our discussion started.

It is well known that many nuclei can be viewed approximately as an axially-deformed rotor. Therefore, it is of practical importance to discuss the case of axial symmetry, for which the description with angular–momentum-projection can be much simpler. If our starting deformed state $|\Phi\rangle$ is axially symmetric, for which the relation $\hat{J}_z|\Phi\rangle = K_0|\Phi\rangle$ holds where K_0 is the conserved K-quantum number, the projection

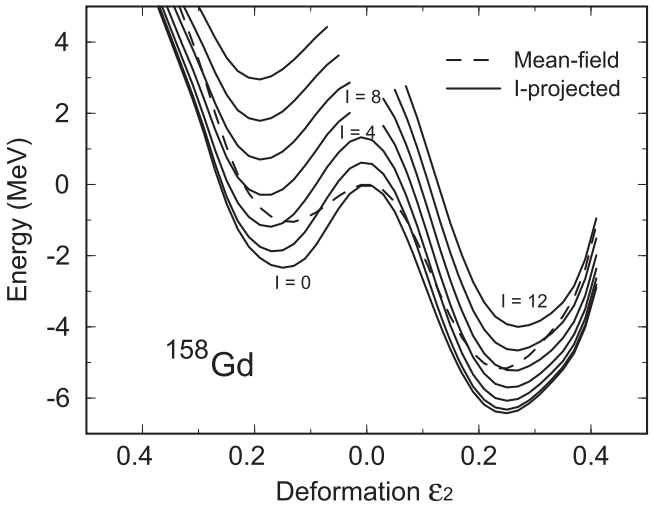

Figure 2. Angular–momentum-projected energy surface calculations for ^{158}Gd for the states with $I = 0$ to $I = 12$ as functions of axial deformation. The unprojected (nonrotating) energies (denoted as mean field) are also shown for comparison. This figure is taken from figure 1 of [47] and reproduced with permission. Copyright APS 2003.

operator $\hat{P}^I_{MK}$ in equation (11) reduces effectively to

$$\left(I + \frac{1}{2}\right)\int_0^{\pi} \mathrm{d}\beta \sin\beta \; d^I_{MK}(\beta)\mathrm{e}^{-\imath\beta\hat{J}_y} \tag{19}$$

since α and γ can be integrated explicitly when evaluating the matrix elements. This is an one-dimensional integration about β with the small-d function [41]. Note for the case of axial symmetry, the form of equations in (16), (17), (18) remains the same as in the general three-dimensional case, except that the projector takes the form of equation (19). The simplest but very useful example is the axially-deformed vacuum state with $K = 0$ of a doubly even nuclei. In this case, there is only one term with $K = K_0$ remains in the summation over K. The solution of (17) then becomes

$$E^I = \frac{H^I_{K_0K_0}}{N^I_{K_0K_0}} \text{ with } F^I_{K_0} = \frac{1}{\sqrt{N^I_{K_0K_0}}}. \tag{20}$$

This represents the most primitive form of the angular–momentum-projection theory in the old days [44–46]. It does not contain admixture of excited configurations and thus can describe only one 'rotational band', whose 'rotational energy' is obtained by evaluating E as a function of spin I.

However, this simple procedure already gives an energy lower than that in equation (6) because the space spanned by $\hat{R}(\Omega)|\Phi\rangle$ is larger than that consisting of just a single state $|\Phi\rangle$ which corresponds to $\Omega = 0$. The energy difference between the unprojected one in equation (6) and the projected one in equation (20) represents the gained correlations by projection. Thus, even from this simplest case, one recognizes that angular–momentum-projection actually does two jobs: it recovers the rotational quantum number violated in the mean field and it brings additional correlations to the variational states.

To see quantitatively the correlation energy gained by the projection, we show the results in figure 2 obtained by the PSM calculation for angular-momentum-projected energy surfaces in ^{158}Gd. The calculation is performed with a schematic Hamiltonian (see section 4) for projected energies of the axially-deformed vacuum state given in equation (20)

$$E^I(\varepsilon) = \frac{\langle\Phi(\varepsilon)|\, \hat{H}\hat{P}^I \,|\Phi(\varepsilon)\rangle}{\langle\Phi(\varepsilon)|\, \hat{P}^I \,|\Phi(\varepsilon)\rangle} \tag{21}$$

by varying the axial deformation parameter ε. It is seen in figure 2 that the lowest energy for a given angular momentum I is well localized at deformations varying from $\varepsilon \approx 0.24$ at $I = 0$ to $\varepsilon \approx 0.28$ at $I = 12$. There are local minima with negative deformations, but they lie at several MeV higher than those with positive deformations. Figure 2 thus indicates that ^{158}Gd is a stably deformed nucleus against rotation, with pronounced energy minimum corresponding to a prolately-deformed shape. The angular–momentum-projected minima lie at deformations that are slightly larger than the unprojected minimum ($\varepsilon \approx 0.23$). The lowest projected energy minimum with $I = 0$ is pushed down roughly by 1.5 MeV as compared to the unprojected one (shown in figure 2 by the dashed curve). This represents the amount of the correlation energy gained by the projection.

4. Choice of deformed basis and the Hamiltonian

The preceding discussion on angular–momentum-projection introduced a method to construct many-body wave functions. To complete a model, one needs to choose a Hamiltonian and define the deformed basis. There are many different types of effective interaction for nuclear structure calculations. Among them, the quadrupole–quadrupole plus pairing ($QQ + P$) interaction [48–52] has been widely applied to describe various nuclear properties, such as excitation energies, moments, transitions, and reaction rates, for a wide range of nuclei in the medium to heavy mass regions. This interaction is represented by two basic components, the pairing and quadrupole forces as the short and long range parts of the interaction, respectively. Dufour and Zuker have shown that any realistic effective interaction is dominated by the $QQ + P$ interaction with the monopole terms [53]. It has been understood that, while the quadrupole and pairing terms take care of the main and smooth part of the structure properties, the monopole terms play important roles for the shell evolution and are often responsible for explaining anomalous behaviors in spectra and transitions. Therefore, for the present pedagogical purpose, it is sufficient to adopt the simple $QQ + P$ force as the main part of the Hamiltonian. Of course, the projection theory itself is independent of the choice of interactions. For a workable model with angular–momentum-projection, it is open to adoption of any realistic forces.

The interaction used here consists of a sum of schematic (i.e. QQ + monopole mairing + quadrupole pairing) forces, which takes the form

$$\hat{H} = \hat{H}_0 - \frac{\chi}{2}\sum_{\mu}\hat{Q}^{\dagger}_{\mu}\hat{Q}_{\mu} - G_M\hat{P}^{\dagger}\hat{P} - G_Q\sum_{\mu}\hat{P}^{\dagger}_{\mu}\hat{P}_{\mu}. \tag{22}$$

The first term represents the harmonic oscillator single-particle Hamiltonian

$$\hat{H}_0 = \sum_\alpha c_\alpha^\dagger \, \varepsilon_\alpha c_\alpha, \tag{23a}$$

$$\varepsilon_\alpha \equiv \hbar\omega \{ N - \kappa [\, 2\mathbf{j}\cdot\mathbf{s} + \mu(\mathbf{l}^2 - \langle \mathbf{l}^2 \rangle)]_{Nj} \}, \tag{23b}$$

where $c_\alpha^\dagger$ and c_α are respectively the single-particle creation and annihilation operator labeled by a set of the spherical harmonic oscillator quantum numbers $\alpha = \{N, j, m\}$. Note that l is known when N and j are specified. The Fermi energy is included in the single-particle energy ($\varepsilon_\alpha \to \varepsilon_\alpha - \lambda$) for convenience. The parameters κ and μ in (23b), which are commonly called Nilsson parameters and can be empirically fitted to experiment, ensure the correct shell structure.

In PSM calculations, the Nilsson parameters are directly adopted from the literature, once for a whole mass region without any modification for individual nuclei. The Nilsson parameters, κ and μ in (23b), are determined so that the resulting single-particle energies reproduce the experimentally-observed levels that characterize the single-particle configurations for a mass region [54]. The N-dependent κ and μ values were later suggested [40, 55] by more careful fitting to a large body of data across the periodic table, from the light to the superheavy mass regions, and become 'standard' in describing the single-particle structure for stable nuclei. Such a phenomenological potential, though having proven to be very successful, has an obvious shortcoming when applied to exotic mass regions where experimental information is lacking. Therefore, modifications of the Nilsson parameters based on very limited experimental data for the ^{132}Sn mass region were first attempted by Zhang *et al* [56]. This shortcoming in the Nilsson model could hamper applications of the PSM in the mass regions far from the stability. We shall comment this later in section 7.

The one-body operators in (22) are defined (for each kind of nucleons) by

$$\hat{Q}_\mu = \sum_{\alpha\beta} c_\alpha^\dagger Q_{\mu\alpha\beta} c_\beta, \tag{24a}$$

$$\hat{P}^\dagger = \frac{1}{2}\sum_\alpha c_\alpha^\dagger c_{\bar{\alpha}}^\dagger, \tag{24b}$$

$$\hat{P}_\mu^\dagger = \frac{1}{2}\sum_{\alpha\beta} c_\alpha^\dagger Q_{\mu\alpha\beta} c_{\bar{\beta}}^\dagger, \tag{24c}$$

where $\bar{\alpha}$ represents the time reversal of α ($c_{\bar{\alpha}} = \hat{T} c_\alpha \hat{T}^\dagger = (-)^{j-m} c_{Nj-m}$) while

$$Q_{\mu\alpha\alpha'} = \delta_{NN'} \, (N\, jm | Q_\mu | N' j' m') \tag{25}$$

is the matrix element of the SU(3) quadrupole generator, whose matrix elements are equal to those of the dimensionless mass quadrupole operator

$$\sqrt{\frac{4\pi}{5}} \left(\frac{r}{b}\right)^2 Y_{2\mu} \tag{26}$$

for $N = N'$ but vanish for $N \neq N'$, with b being the harmonic oscillator length

$$b^2 = \frac{\hbar}{m\omega}. \tag{27}$$

Note the symmetry properties of the matrix element

$$Q_{\bar{\mu}\alpha\beta} \equiv Q_{\mu\bar{\alpha}\bar{\beta}} = Q_{\mu\beta\alpha} = (-)^\mu Q_{-\mu\alpha\beta}, \tag{28}$$

which ensure the relations $\hat{Q}_{\bar{\mu}} \equiv \hat{T}\hat{Q}_\mu\hat{T}^\dagger = \hat{Q}_\mu^\dagger = (-)^\mu \hat{Q}_{-\mu}$.

The HFB single-particle Hamiltonian resulting from (22) is

$$\hat{H}_{\rm HFB} = \hat{H}_0 - \chi \sum_\mu \langle \hat{Q}_\mu \rangle \hat{Q}_\mu - G_{\rm M} \langle \hat{P} \rangle (\hat{P} + \hat{P}^\dagger) - G_{\rm Q} \sum_\mu \langle \hat{P}_\mu \rangle (\hat{P}_\mu + \hat{P}_\mu^\dagger). \tag{29}$$

Here, $\langle \cdots \rangle$ means the expectation value with respect to the HFB vacuum state $|0\rangle$.

We can adjust the nuclear size by using the conventional harmonic oscillator parameters

$$\omega_\tau = \omega_0 \, a_\tau, \;\; b_\tau^2 = \frac{b_0^2}{a_\tau}, \tag{30a}$$

$$b_0^2 = \frac{\hbar}{m\omega_0}, \;\; a_\tau \equiv \left\{ 1 \pm \frac{N-Z}{A} \right\}^{\frac{1}{3}} \tag{30b}$$

with + (–) for τ = neutron (proton). If we use the value $\hbar\omega_0 = 41.4678 A^{-\frac{1}{3}}$ MeV, for example, we find $b_0^2 = A^{\frac{1}{3}}$ fm^2.

In equation (29), there are three coupling constants, χ for the QQ force, and $G_{\rm M}$ and $G_{\rm Q}$ for the monopole- and quadrupole-pairing force, respectively. For simplicity, both pairing-type forces are assumed to act only between like nucleons (i.e. the isovector type). The coupling constant for the monopole pairing force, $G_{\rm M}$, is taken as

$$G_{\rm M} = \left(G_1 \mp G_2 \frac{N-Z}{A} \right) \frac{1}{A} \;\; ({\rm MeV})$$
$$\text{with} \;\; - \;\; (+) \text{ for neutron (proton)}, \tag{31}$$

where G_1 and G_2 are adjusted to yield the known odd-even mass differences. Another simpler form for the monopole pairing force would be $G_{\rm M} = G_\tau/A$ (τ = neutron and proton), which does not contain the isotopic dependence. For the quadrupole pairing force, we assume that the strength $G_{\rm Q}$ is simply proportional to $G_{\rm M}$ with an overall constant γ

$$G_{\rm Q} = \gamma \; G_{\rm M}. \tag{32}$$

For PSM calculations, γ is usually fixed by choosing a value around 0.20 (in practice, from 0.15 to 0.25).

The strength of the QQ force is related to the quadrupole deformation parameter as follows. The second term in right-hand side of equation (29) may be identified as the (stretched) Nilsson potential $\frac{2}{3}\varepsilon\hbar\omega\hat{Q}_0$. Introducing $x_\tau \equiv \hbar\omega_\tau \langle \hat{Q}_0 \rangle_\tau$ and $C_{\tau\tau'} \equiv \chi_{\tau\tau'} (\hbar\omega_\tau \hbar\omega_{\tau'})^{-1}$, one obtains the self-consistent condition

$$C_{nn}\, x_n(\varepsilon_n, \varepsilon_p) \;+\; C_{np}\, x_p(\varepsilon_n, \varepsilon_p) = \frac{2}{3}\varepsilon_n, \tag{33a}$$

$$C_{pn}\, x_n(\varepsilon_n, \varepsilon_p) \;+\; C_{pp}\, x_p(\varepsilon_n, \varepsilon_p) = \frac{2}{3}\varepsilon_p, \tag{33b}$$

whose solutions ε_n and ε_p are in general different from each other. We assume as usual that the neutron and proton deformation parameters are equal to each other, $\varepsilon_n = \varepsilon_p \equiv \varepsilon$. The necessary and sufficient condition for this to be true is that two equations of (33) reduce to a single equation, namely they have to be linearly dependent

$$C_{nn}C_{pp} - C_{np}^2 = 0 \; (C_{pn} = C_{np}), \tag{34}$$

which is the condition for the determinant of (33) to vanish, so that (33) and (34) lead to the iso-scalar coupling $C_{nn} = C_{pp} = C_{np}$. We therefore obtain the relation

$$\chi_{\tau\tau'} = \frac{\frac{2}{3}\varepsilon\ \hbar\omega_\tau\ \hbar\omega_{\tau'}}{\hbar\omega_n\langle\hat{Q}_0\rangle_n \;+\; \hbar\omega_p\langle\hat{Q}_0\rangle_p}. \tag{35}$$

This is a very useful relation since the nuclear deformation is a well studied quantity [57]. The QQ force coupling constant corresponding to a given deformation parameter ε is thus obtained by (35). We adopt this strategy to ensure that the QQ force generates the correct (axial) deformation, and any departure from the relation (35) will reduce the quality of the model [58]. Note, however, that $\chi_{\tau\tau'}$ remains undetermined for $\varepsilon = 0$ (a spherical nucleus) since both $\langle\hat{Q}_0\rangle_n$ and $\langle\hat{Q}_0\rangle_p$ vanish.

The single-particle space for the PSM is large, which usually includes three (four) major harmonic oscillation shells each for neutrons and protons in a calculation for deformed (superdeformed), heavy nuclei. The use of such a large size of single-particle space ensures that the collective motion is defined microscopically by accommodating a sufficiently large number of active nucleons. This is in a sharp contrast to conventional shell models based on the spherical basis, which is normally confined in one harmonic oscillation shell.

This force model works surprisingly well despite its simplicity. It is therefore sufficient to use it in the present paper for presentation of the projection theory. Nevertheless, depending on problems, this might be too restrictive and one will have to introduce (schematic) forces of a more general type. For example, the neutron–proton interaction is present only in the (particle-hole type) QQ force in (22). As the force is of the separable form, one can easily supply additional terms to it. In [59], the two-body octupole–octupole and hexadecupole–hexadecupole forces were introduced to the Hamiltonian (22) to obtain necessary correlations for specific qp configurations. In the study of β-decay and electron-capture rates, the Gamow–Teller force of the charge-exchange terms must be included [60]. This term is a charge-dependent separable interaction with both particle-hole (ph) and particle-particle (pp) channels [61], which act between protons and neutrons.

Summarizing the logical structure of the model, the calculation proceeds in the following sequence. For each nucleon, one first diagonalizes the Nilsson Hamiltonian

$$\hat{H}_N = \hat{H}_0 - \frac{2}{3}\hbar\omega\left\{\varepsilon\hat{Q}_0 + \varepsilon'\frac{\hat{Q}_{+2} + \hat{Q}_{-2}}{\sqrt{2}}\right\} \tag{36}$$

with given deformation parameters ε and ε'. For the axial deformation ε, we know it either through the connection with the experimental transition rate of electric quadrupole and the spectroscopic quadrupole moment [62], or from theoretical calculations [57]. The triaxial deformation ε', however, is treated as an adjustable parameter, except for some cases ε' may represent the deformation minimum in the projected energy surface. $\hat{H}_0$ in equation (36) is the spherical single-particle Hamiltonian containing the proper spin–orbit force for correct shell closures [20]. For the case of axial symmetry, $\varepsilon' = 0$, and the second term in the brace of equation (36) vanishes. One then carries out the usual BCS procedure to take the (monopole) pairing force into account. This defines the Nilsson+BCS qp basis. The strength of the QQ force can be evaluated by the relation (35). This fixes the Hamiltonian (22), which is then diagonalized within the shell model space spanned by a selected set of configurations (see next section).

In the projection theory, the effect of the rotation is fully described by the projection operator and the whole dependence of the wavefunctions on spin is contained in the eigenvectors since the qp basis is spin independent. This feature makes not only the numerical treatment simple and stable but also the interpretation of the result easy and intuitive. Now the central task is to evaluate various projected matrix elements efficiently. All the relevant technical details will be given in appendix. The early version of the codes with all the matrix element computation was published in [63].

5. Truncation of the shell-model space

Investigation in nuclear structure physics has been mainly concentrated on two aspects: the collective motion and single particle excitation, and more importantly, the interplay between them. The nuclear shell model can in principle include both aspects and describe the interplay. However, as discussed above, the shell model calculation can be applied only to a small range of nuclei in the nuclear chart. Moreover, even that a shell model reproduces data nicely, one often interprets the physics with additional help of the mean-field models [30]. This is because a shell-model state is presented by numerous number of basis states that do not correspond to physical states. It is therefore conceptually interesting and practically useful if one can represent the nuclear states with good physical algorithms.

As we have seen, the basic concept of angular–momentum-projection is diagonalization of the full many-body Hamiltonian in the subspace spanned by a set of generating functions $\hat{R}(\Omega)|\Phi\rangle$, which depend on the continuous parameters Ω. This space is usually called the 'collective space' [2], and the resulting states are collective in nature.

We note that the final wavefunction with angular–momentum-projection, $|\Psi\rangle$ of equation (16), is written as a

summation of the states labeled by K. Thus there is a possibility that one generalizes it to express the shell-model wavefunction as a linear combination of (angular–momentum) projected states with various kinds of configurations. These configurations, denoted by κ in the following, may include collective ones as well as those of qp excitations, and all these are mixed by diagonalization of residual interactions. In this way, we approach the full shell-model problem in a subspace characterized by collective and qp excitations. In this practice, one has a freedom to select the configurations to be contained in the diagonalization procedure, or equivalently to say, to truncate the shell-model space under the physical guidance.

Let us start with a simple example. If $a^\dagger_\nu$ and $a^\dagger_\pi$ are the qp creation operators, with the index ν_i (π_i) denoting the neutron (proton) quantum numbers and running over properly selected single-qp states, and $|\Phi\rangle$ the corresponding qp vacuum, the projected multi-qp bases $\{|\Phi_\kappa\rangle\}$ for even–even nuclei are given as follows:

$$\{\hat{P}^I_{MK}\ |\Phi\rangle,\ \hat{P}^I_{MK}a^\dagger_{\nu_i}a^\dagger_{\nu_j}\ |\Phi\rangle,\ \hat{P}^I_{MK}a^\dagger_{\pi_i}a^\dagger_{\pi_j}\ |\Phi\rangle,\ \hat{P}^I_{MK}a^\dagger_{\nu_i}a^\dagger_{\nu_j}a^\dagger_{\pi_k}a^\dagger_{\pi_l}\ |\Phi\rangle,\ \ldots\}. \tag{37}$$

In the bases (37), '…' denotes those configurations that contain more than two like-nucleon quasiparticles. These high-order qp configurations have higher excitation energies due to mutual Pauli blocking of levels. If the configurations denoted by '…' in (37) were completely included, one would recover the full shell model space written in the representation of qp excitation. The above concept can be considered as a kind of Tamm–Dancoff approximation [2] to which the so-called broken-pair approximation [64] also belongs.

For the basis states presented in (37), shell-model truncation can now be implemented by simply excluding the states of high-order quasiparticles with higher energies. We can do this because, by using deformed bases, we know clearly which configurations are low in energy. Usually, configurations constructed by combinations from only a few orbitals around the Fermi surfaces are sufficient for a description of the low-energy qp excitations. The truncation is thus so efficient that dimension never poses a problem even for a description of superdeformed nuclei [65, 66] or superheavy nuclei [67, 68].

Similarly, we can select a set of multi-qp states $\{|\Phi_\kappa\rangle\}$ which we want to take into account in the shell-model space for other types of nuclei, i.e. odd-neutron, odd-proton, and doubly-odd nuclei. These multi-qp bases can be written, respectively, as

$$\begin{aligned}
&\{\hat{P}^I_{MK}a^\dagger_{\nu_i}\ |\Phi\rangle,\ \hat{P}^I_{MK}a^\dagger_{\nu_i}a^\dagger_{\pi_j}a^\dagger_{\pi_k}\ |\Phi\rangle,\ \hat{P}^I_{MK}a^\dagger_{\nu_i}a^\dagger_{\nu_j}a^\dagger_{\nu_k}\ |\Phi\rangle,\ \ldots\},\\
&\{\hat{P}^I_{MK}a^\dagger_{\pi_i}\ |\Phi\rangle,\ \hat{P}^I_{MK}a^\dagger_{\pi_i}a^\dagger_{\nu_j}a^\dagger_{\nu_k}\ |\Phi\rangle,\ \hat{P}^I_{MK}a^\dagger_{\pi_i}a^\dagger_{\pi_j}a^\dagger_{\pi_k}\ |\Phi\rangle,\ \ldots\},\\
&\{\hat{P}^I_{MK}a^\dagger_{\nu_i}a^\dagger_{\pi_j}\ |\Phi\rangle,\ \hat{P}^I_{MK}a^\dagger_{\nu_i}a^\dagger_{\nu_j}a^\dagger_{\nu_k}a^\dagger_{\pi_l}\ |\Phi\rangle,\\
&\hat{P}^I_{MK}a^\dagger_{\nu_i}a^\dagger_{\pi_j}a^\dagger_{\pi_k}a^\dagger_{\pi_l}\ |\Phi\rangle,\ \ldots\},
\end{aligned} \tag{38}$$

if one allows up to three like-nucleon quasiparticles in a configuration. Again, if the configurations denoted by '…' in the above expressions were completely included, one would recover the full shell model space written in the representation of qp excitation for the respective types of nuclei.

Once the qp basis $\{|\Phi_\kappa\rangle\}$ is prepared, one diagonalizes the Hamiltonian in the shell-model space spanned by $\{\hat{P}^I_{MK}|\Phi_\kappa\rangle\}$. This leads to the eigenvalue equation

$$\sum_{\kappa'K'}\{H^I_{\kappa K\,\kappa'K'} - EN^I_{\kappa K\,\kappa'K'}\}\ F^I_{\kappa'K'} = 0 \tag{39}$$

with the normalization condition

$$\sum_{\kappa K\kappa'K'} F^I_{\kappa K}N^I_{\kappa K\,\kappa'K'}F^I_{\kappa'K'} = 1. \tag{40}$$

Equations (39) and (40) are the straightforward generalization of (17) to a multi-configuration space. The Hamiltonian and norm elements are defined respectively by

$$H^I_{\kappa K\,\kappa'K'} = \langle\Phi_\kappa|\hat{H}\hat{P}^{\,I}_{KK'}|\Phi_{\kappa'}\rangle, \tag{41a}$$

$$N^I_{\kappa K\,\kappa'K'} = \langle\Phi_\kappa|\hat{P}^{\,I}_{KK'}|\Phi_{\kappa'}\rangle, \tag{41b}$$

which is the generalization of (18). After solving the eigenvalue equation (39), we obtain the normalized eigenstate

$$|\Psi_{IM}\rangle = \sum_{\kappa K}F^I_{\kappa K}\hat{P}^I_{MK}|\Phi_\kappa\rangle, \tag{42}$$

which is the generalization of (16).

5.1. Basis with axial symmetry

The presence of axial symmetry simplifies the equations and numerical calculations. In particular, axial symmetry implies that the set of quantum numbers κ in the summations contains, amongst other labels, the total intrinsic magnetic quantum number K implicitly. Therefore, the summations over K in equations (39)–(42) may be omitted since only one specific K contributes to the sum for a given κ. This leads to the set of equations

$$\sum_{\kappa'}\{H^I_{\kappa\kappa'} - EN^I_{\kappa\kappa'}\}\ F^{\,I}_{\kappa'} = 0, \tag{43a}$$

$$\sum_{\kappa\kappa'}F^I_\kappa N^I_{\kappa\kappa'}F^{\,I}_{\kappa'} = 1, \tag{43b}$$

with

$$H^I_{\kappa\kappa'} = \langle\Phi_\kappa|\hat{H}\hat{P}^{\,I}_{KK'}|\Phi_{\kappa'}\rangle, \tag{44a}$$

$$N^I_{\kappa\kappa'} = \langle\Phi_\kappa|\hat{P}^{\,I}_{KK'}|\Phi_{\kappa'}\rangle. \tag{44b}$$

As in this case, the index κ always means a basis state with a certain K, solving for the eigenvalue equation (43) can be said to carrying out K-mixing [69].

Deformed bases with axial symmetry describe many nuclei that are understood to have a stable (prolately or oblately deformed) shape. Microscopic descriptions for the rotational motion of a stably-deformed nucleus involve coherent contributions from many nucleons. The yrast state is of particular interest because it carries valuable information of how the nucleons are organized in the lowest energy state for

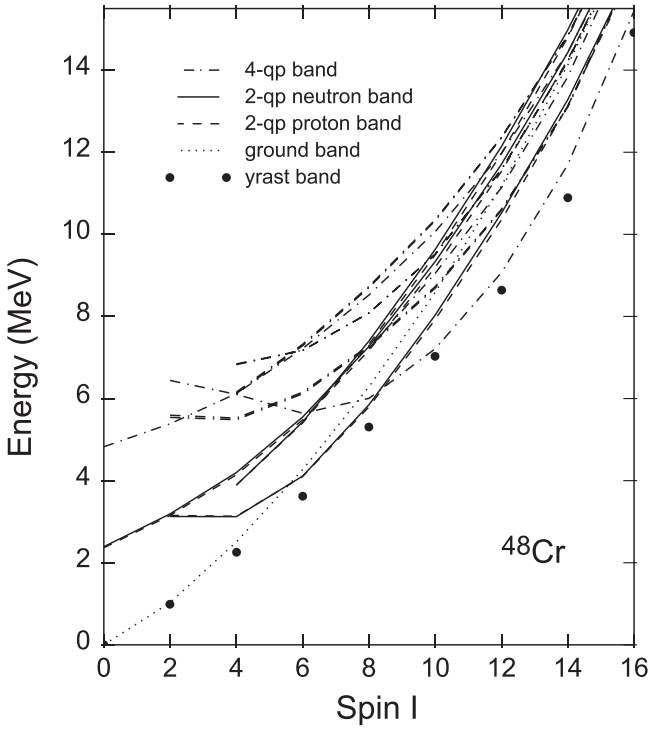

Figure 3. Diagram of angular–momentum-projected bands from the PSM calculation for ^{48}Cr. This figure is taken from figure 3 of [31] and reproduced with permission. Copyright APS 1991.

a given angular momentum and how the organization responds to the rotation. In the ground state, nuclei tend to couple their nucleons pairwise. The (angular–momentum) projected qp vacuum state $\hat{P}^{I}_{MK}\,|\Phi\rangle$, the first term in (37), describes the rotational behavior of the ground band in a deformed nucleus. As the nucleus rotates, the Coriolis force, acting on the nucleon pairs in the intrinsic rotating frame, can break the pairs and thus destroy the nuclear superfluidity [70]. A sudden increase in moment of inertia at a given angular momentum is usually an indication of the pair breaking with their spins of the nucleons aligned along with the axis of rotation [71]. The projected 2-qp configurations in (37) describe such spin-aligned states [22]. Mixing of the projected qp vacuum and projected 2-qp states through diagonalization describes the interplay between the collective ground state and the spin-aligned ones. In this way, the experimentally-observed backbending in moment of inertia in many well-deformed nuclei can be described microscopically [72].

Backbending in moment of inertia in deformed nuclei is an indication for the structure changes in a rotational band mainly due to the interplay between the fully-paired ground state and spin-aligned states. This can be visualized in a diagram consisting of energies of various configurations as functions of angular momentum. The band diagram obtained from the PSM calculation for ^{48}Cr [31] is shown in figure 3, where different types of curves distinguish different configurations and the filled circles represent the yrast states obtained after the configuration mixing, which are compared with the experimental data [29] in figure 1. Among several 2-qp bands which start at energies of 2–3 MeV, two of them (one solid and one dashed curve) cross the ground band at spin 6. They are neutron 2-qp and proton 2-qp bands consisting of two $f_{7/2}$ quasiparticles of $\Omega = 3/2$ and $5/2$ coupled to total $K = 5/2 - 3/2 = 1$. It is noticed that the crossing angle is relatively small so that the yrast band smoothly changes its structure from the 0-qp to the 2-qp states around spin $I = 6$. Therefore, no clear effect of this (first) band crossing is seen in the yrast band (see figure 1) and it is thus not the reason for the observed band disturbance.

The above two ($K = 1$) 2-qp bands can combine to a ($K = 2$) 4-qp band which represents simultaneously broken neutron and proton pairs. This 4-qp band (one of the dashed–dotted curves which becomes the lowest band for $I \geqslant 10$ in figure 3) shows a unique rotational behavior as a function of spin. As spin increases, it goes down first but turns up at spin $I = 6$. This behavior has its origin in the spin alignment of a decoupled band as intensively discussed in [21]. Because of this, it can sharply cross the 2-qp bands between spin $I = 8$ and 10 and becomes the lowest band thereafter. The yrast band gets the main component from this 4-qp band starting from $I = 10$. This is seen in the band diagram as a (second) band crossing. Thus, we can interpret the backbending in ^{48}Cr as a consequence of the simultaneous breaking of the $f_{7/2}$ neutron and proton pairs, thus giving a clear physical picture about the experimentally-observed band disturbance in this nucleus [29]. The simultaneous breaking of the $f_{7/2}$ neutron and proton pairs in the PSM corresponds to a simultaneous excitation of two neutrons and two protons to the $f_{7/2}$ orbit in the spherical shell model language.

In addition to the above study, angular–momentum-projection on deformed bases with axial symmetry provides a useful tool for understanding the so-called K-isomer. K-isomer is an excited nuclear state, in which the larger K quantum number inhibits its decay to other lower-K states due to the selection rules, and endows the isomeric state with a lifetime that can be much longer than most nuclear states [73]. The condition for the formation of K-isomers is the existence of high j, high Ω orbitals near the Fermi surfaces, which can couple to form high-K states by two or more quasiparticles [59, 74, 75]. Physically, these are precisely the basis states with the axial symmetry labeled with K. Once the high-K states are built in the model space, diagonalization will be responsible for the K-mixing, and thus the underlying mechanism for the so-called K-violation [73] is described microscopically in the angular–momentum-projection theory.

K-isomers in superheavy elements are thought as stepping stones towards the possible island of stability because their structure is relevant to the positions of the high-j single-particle orbits, which are the key ingredient in the prediction for the existence of the island [76]. With a good reproduction by the PSM calculation, the experimentally-observed 184 μs isomer at 2.5 MeV of excitation in the $Z = 102$ and $N = 152$ nucleus ^{254}No was interpreted [77] to be of a 4-qp structure with total $K = 16$, which carries valuable structure information on four different high-j single-particle orbitals (two for neutrons and two for protons).

5.2. Basis with triaxiality

There are many other nuclei that do not exhibit an axial-rotor behavior near the ground state, even not approximately. Likely, these nuclei either have an axially asymmetric shape or are soft without a well-defined shape. Gao *et al* have pointed out [78] that triaxiality is a more general effect in nuclei as previously thought. For these nuclei, the above discussed basis with axial symmetry is no longer efficient. One way to describe these nuclei is to introduce an additional degree of freedom in the basis that breaks the axial symmetry. One thus ends up with a triaxially-deformed basis including both axial and triaxial deformations, described by parameters ε and ε' in equation (36). One should keep in mind that in this case, the intrinsic states $|\Phi_\kappa\rangle$, for example those in (37), have no restriction in the Euler space, and therefore, the angular–momentum-projection should be carried out in the three-dimensional space. For the eigenvalue equations one should therefore use the general forms given in equations (39) and (40).

It is important to note that for the case of axial symmetry, the qp vacuum state has $K = 0$, whereas, in the case with triaxial deformation, the vacuum state is a superposition of all possible K-values. Rotational bands built based on the triaxial-basis states are obtained by specifying different values for the K-quantum number appearing in the general angular-momentum projector in equation (11). The allowed values of the K-quantum number for a given intrinsic state are determined through the following symmetry consideration. Applying the symmetry operator $\hat{S} = \mathrm{e}^{-\imath\pi\hat{J}_z}$, we have

$$\hat{P}^I_{MK}\ |\Phi\rangle = \hat{P}^I_{MK}\hat{S}^\dagger\hat{S}\ |\Phi\rangle = \mathrm{e}^{\imath\pi(K-\kappa)}\hat{P}^I_{MK}\ |\Phi\rangle. \qquad (45)$$

For the self-conjugate vacuum or 0-qp state, $\kappa = 0$ and, therefore, it follows from the above equation that only $K=$ even values are permitted for this state. For 2-qp states, $a^\dagger a^\dagger\ |\Phi\rangle$, the possible values for K-quantum number are both even and odd, depending on the structure of the qp state. For example, for a 2-qp state formed from the combination of the normal and the time-reversed states $\kappa = 0$, only $K =$ even values are permitted. For the combination of the two normal states, $\kappa = 1$ and only $K=$ odd states are permitted.

This additional symmetry breaking in the deformed basis (i.e. breaking of axial symmetry) coupled with the full three-dimensional angular–momentum-projection brings significant effects to the calculation. We mention two examples. It was shown [79] that the three-dimensional angular–momentum-projection from a triaxial Nilsson+BCS deformed intrinsic wave function is essential for a description of the low-spin states in transitional nuclei such as ^{156}Er, ^{158}Yb, ^{176}W, and ^{184,186,188}Os. The moments of inertia of these nuclei depict a steep increase as functions of the rotational frequency in the region $I < 10$, indicating a rapid shape change with rotation, and this can be explained only when a triaxially deformed basis with γ-deformation of $\gamma \approx 30°$ is assumed in the basis [79]. Using the relation $\tan\gamma = \varepsilon'/\varepsilon$, $\gamma = 30°$ corresponds to the deformation ratio $\varepsilon'/\varepsilon \approx 0.58$.

The breaking of additional symmetry in the shell-model basis results in a much richer spectrum than the case that is restricted to axial symmetry. Since the qp vacuum state $|\Phi\rangle$ is a mixture of K states, one can project it to all possible K. Taking a deformed doubly-even nucleus as another example, according to equation (45), all $K=$ even values satisfying $K \leqslant I$ are permitted for the 0-qp vacuum state. Therefore, applying the projection operator to the 0-qp vacuum state, one obtains, beside of the $K = 0$ ground band (g-band), also the bands belonging to $K = 2, 4, \ldots$. These $K \neq 0$ bands should lie, theoretically, at the infinity when the triaxial deformation (denoted by ε') is set to zero (i.e. the case with the axial symmetry), but come down in energy with nonzero ε'.

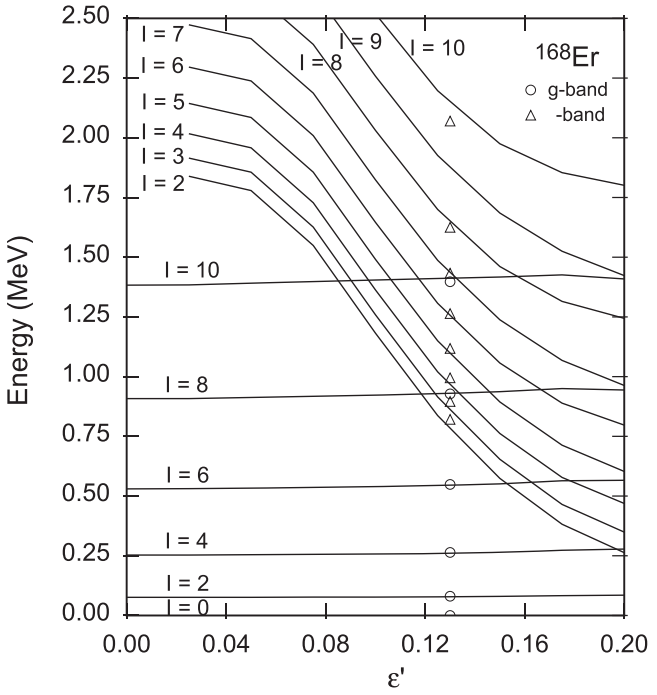

Figure 4. Calculated energies (solid lines) of the g- and γ-band in ^{168}Er as functions of triaxiality parameter ε' for angular momenta up to $I = 10$. The experimental g-band (open circles) and γ-band (open triangles) are best reproduced by the TPSM at $\varepsilon' = 0.13$. This figure is taken from figure 1(a) of [80] and reproduced with permission. Copyright APS 2000.

Let us consider a well-deformed nucleus ^{168}Er, which is generally considered to be an axially symmetric nucleus. Figure 4 shows the calculated energies as functions of the triaxiality parameter ε' for angular momenta up to $I = 10$. In addition to the usual g-band with spins $I = 0, 2, 4, \ldots$, a new set of rotational states with spins $I = 2, 3, 4, \ldots$ appears [80]. One sees from figure 4 that, for the g-band of ^{168}Er, the energies as functions of triaxiality are nearly flat and their values remain close to those at zero triaxiality. Thus, the triaxial basis has no effect on the g-band for a well-deformed nucleus and does not destroy the good g-band result obtained with an axially deformed basis.

However, it has a drastic effect on excited bands (second and higher excited bands are not shown in the figure) which lie at very high energy when $\varepsilon' = 0$. As seen in figure 4, their excitation energies come down quickly as ε' increases. At $\varepsilon' = 0.13$, the first excited band reproduces the experimentally observed γ-band in ^{168}Er (while preserving the good

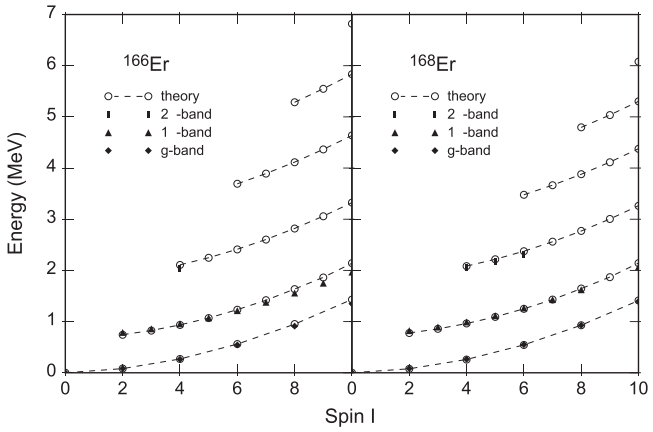

Figure 5. The spectra up to $I = 10$ for ^{166,168}Er. Theoretical results are compared with the available experimental data for the g-band and γ-band, as well as the 4^+ 2γ-band in ^{166}Er and ^{168}Er. This figure is taken from figure 2 of [80] and reproduced with permission. Copyright APS 2000.

g-band agreement). It should be noted that the excited bands discussed here are obtained by introducing triaxiality in the basis (i.e. the qp vacuum). They are collective excitations, but not qp excitations. We may thus identify the first excited band as the collective γ-band, the second excited band as the 2γ-band, the third excited band as the 3γ-band, etc.

In figure 5, we plot all the states for spins $I \leqslant 10$ obtained after diagonalization within our projected triaxial basis for the two isotopes ^{166,168}Er in which a 2γ-band has been reported by experimental observations. For both isotopes, the second excited theoretical band agrees beautifully with the experimental 4^+ 2γ-band. Since our theory agrees very well with the g-band and the (1-phonon) γ-band observed in these nuclei, the present results support strongly the interpretation of these data as 2γ-bands [80]. The effects of breaking the axial symmetry with three-dimensional angular–momentum-projection can also be seen in the study of electromagnetic properties (BE(2) and g factor) [81–83].

The above two examples about the enriched shell-model basis with both axial and triaxial quadrupole-deformations simultaneously improve the results of the g-bands in transitional nuclei and lead to a consistent description of multi-phonon γ-bands in both transitional and well-deformed nuclei. The resulting g- and multi-phonon γ-bands agrees surprisingly well with the existing data, even though we have used the simplest possible configuration space (i.e. triaxially-deformed qp vacuum state). We thus see again the efficiency of the properly chosen deformed states for shell-model calculations. We note that two deformation parameters are involved for determination of the basis. We have relatively good knowledge on the axial deformation ε through its connection with the experimental transition rate of electric quadrupole and the spectroscopic quadrupole moment [62]. The triaxial deformation ε', however, is treated here as a free parameter, except for some cases ε' may coincide with a deformation minimum in the projected energy surface.

Further expanding the basis, one includes qp configurations associated with the triaxially-deformed vacuum. Inclusion of multi-qp states in a triaxially-deformed well results in more fruitful band structures, and in particular the interplay between the collective motion and qp excitations in a triaxially-deformed well can be discussed. This is because with triaxiality in the basis, a single configuration contains a rich mixture of many possible K-states and after angular–momentum-projection, each one of them corresponds to a rotational band. Such an extended model is called the triaxial projected shell model (TPSM).

The TPSM approach was employed to study the high-spin band structures of the Er isotopes from $A = 156$ to 170 [84]. The qp states considered are 0-qp, 2-qp neutron and 2-qp proton states, and the 4-qp state. Interesting features of the results obtained in this approach are: (i) γ bands are quite close to the yrast line for the neutron deficient Er isotopes, in particular, for ^{156}Er and ^{158}Er. It is further evident that these γ states become even lower in energies for high-spin states. For ^{156}Er and ^{158}Er, they become lower than the ground-state band for $I > 14$. It was proposed that this is a feature of γ-soft nuclei [84]. (ii) γ bands are pushed up in energy with increasing neutron number along the isotopic chain, and further the degree of anharmonicity of γ vibration also increases. (iii) The wave function decomposition of the bands demonstrates that for neutron-deficient Er isotopes, there is a significant mixture of the γ configuration in the ground-state band and vice versa. The neutron-rich ^{170}Er nucleus, in contrast, has the intrinsic structures expected for a well-deformed nucleus with the ground-state band comprising a nearly pure $K = 0$ configuration.

Multi-qp band-structures in some neutron-deficient Ce- and Nd-isotopes were also studied [85]. It was shown that γ-band built on the 2-qp configurations can modify the band-crossing features in these nuclei. The 2-qp γ-band with $K = 3$ are shown to be energetically favored for some angular-momentum states and form the first excited bands in nuclei studied in [85]. The same approach was also extended to odd-proton systems with the inclusion of projected one- and three qp configurations in the shell model space. Consequently, γ- and 2γ-bands in the odd-proton nucleus ^{103}Nb were studied as an example [86]. It was demonstrated that the observed yrast- and γ-bands in ^{103}Nb are reproduced quite well by the TPSM approach.

5.3. Basis with both quasiparticle and phonon excitations

The above description for γ vibrational states was based on a shell-model concept by introducing a triaxially-deformed basis coupled with three-dimensional angular–momentum-projection. In addition to γ-vibration, the low-energy collective motion in nuclei is characterized also by β-vibration. Unlike the phonon model based on phonon excitations [87], 0^+ collective excited states are not built in the above projection calculation. In principle, the collective 0^+ states can emerge in a shell-model calculation if one would include many $K^\pi = 0^+$ multi-qp states on top of the qp vacuum configuration. However, since the states constructed in this way are mainly qp in character, the collectivity of such a 0^+ excited state is generally expected to be weak. To describe

these vibrations efficiently, one may borrow the phonon concept and introduce the collective phonon states as components in the total wavefunction (42).

Following this idea, the PSM basis was extended by including not only qp excitations but also collective phonon excitations in the basis. This more general model constructed in a multi-shell basis, which explicitly contains all known types of excitations (the β- and γ-excitations and qp excitations plus rotational states on top of these configurations), is termed heavy shell model [88]. For even–even nuclei the extended basis becomes

$$\{|\Phi_\kappa\rangle\} = \{|\Phi\rangle,\ a^\dagger_{\nu_i}a^\dagger_{\nu_j}|\Phi\rangle,\ a^\dagger_{\pi_k}a^\dagger_{\pi_l}|\Phi\rangle, \\ a^\dagger_{\nu_i}a^\dagger_{\nu_j}a^\dagger_{\pi_k}a^\dagger_{\pi_l}|\Phi\rangle,\ D^\dagger_0|\Phi\rangle,\ D^\dagger_2|\Phi\rangle\}. \quad (46)$$

The total wavefunction is then written as

$$|\Psi^\sigma_{I,M}\rangle = \sum_{K,\kappa} F^{I,\sigma}_{K,\kappa}\hat{P}^I_{MK}|\Phi_\kappa\rangle, \quad (47)$$

where σ denotes different eigen-states of same angular momentum and κ an intrinsic state in (46).

In the basis (46), there are collective pair operators, $D^\dagger_0$ and $D^\dagger_2$. Projection on states with these D-pairs is supposed to give rise to β and γ bands

$$|\Psi_{I,M}\rangle_\beta = \hat{P}^I_{M0}D^\dagger_0|\Phi\rangle, \quad |\Psi_{I,M}\rangle_\gamma = \hat{P}^I_{M2}D^\dagger_2|\Phi\rangle, \quad (48)$$

where $|\Phi\rangle$ is the usual BCS vacuum (of axial symmetry, for simplicity). Thus these D-pairs may be viewed as collective phonons [88]. Furthermore, combination of two D-pairs can give rise to two-phonon states. For example, $\hat{P}^I_{M0}D^\dagger_2D^\dagger_2|\Phi\rangle$ corresponds to the $K = 0$ 2γ state. In [89], the D_0 (D_2)-pair was suggested to be the linear combination of all the 2-qp states with $K^\pi = 0^+$ ($K^\pi = 2^+$) in the PSM multi-major-shell truncated space. The structure of D-pairs is written as follows:

$$D^\dagger_0 = \sum_{\rho,\mu} f^{K=0}_{\rho\mu}[a^\dagger_\rho a^\dagger_\mu]^{K=0}, \quad D^\dagger_2 = \sum_{\rho,\mu} f^{K=2}_{\rho\mu}[a^\dagger_\rho a^\dagger_\mu]^{K=2}, \quad (49)$$

where $[a^\dagger_\rho a^\dagger_\mu]^K$ is the 2-qp creation operator with $K = 0$ or 2. ρ and μ are the qp state index, and $f^K_{\rho\mu}$ is the structure amplitude, which are determined by diagonalizing the Hamiltonian in the full 2-qp basis with given K.

Thus using the projected basis spanned by (46), one can describe the collective β- and γ-bands, as well as various bands of qp excitations on an equal footing. Diagonalization describes the interplay between them. Examples of application can be found in [90, 91]. The energy scheme of ^{232}U is given in figure 6 as an example. It can be seen that the calculation well reproduces the ground band, β- and γ-bands. According to the calculation, five 2-qp rotational bands emerge at 960 keV, 1367 keV, 1587 keV, 1481 keV and 1487 keV with $K^\pi = 0^+$, 3^+, 4^+, 6^+, and 7^+, respectively. A low-lying 4-qp rotational band with 0^+ is predicted at 2520 keV with the configuration $\frac{7}{2}^-[743]_\nu - \frac{7}{2}^-[743]_\nu + \frac{5}{2}^-[523]_\pi - \frac{5}{2}^-[523]_\pi$.

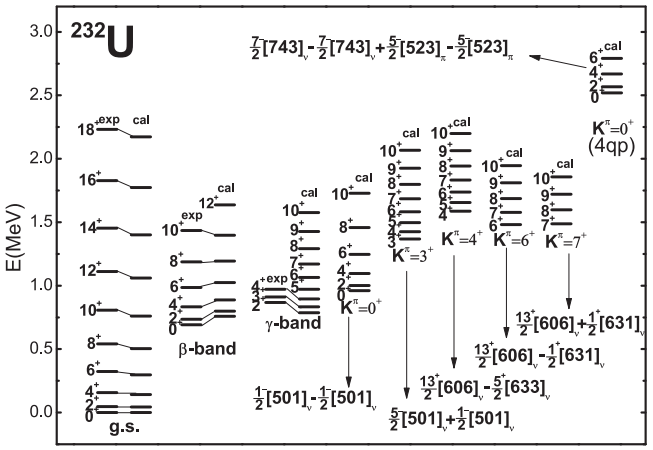

Figure 6. Comparison of the calculated and experimental g-bands, β- and γ-band of ^{232}U. Some 2-qp and 4-qp rotational bands are also given as a theoretical prediction. This figure is taken from figure 4 of [91] and reproduced with permission. Copyright APS 2014.

6. Angular momentum projection in other fields

The rotational symmetry-restoration method discussed in the present paper provides a way to identify the main configurations of interest, and use these as a guidance to truncate the full model space. The method may therefore be generally applied beyond nuclear physics [92]. There have been examples for application of this technique in condensed matter physics [93] and quantum chemistry [94, 95], especially for describing electronic states in the Hubbard model [96, 97]. Using the broken-symmetry solutions of the HFB theory, the method of restoration of broken symmetries has been proven particularly efficient for an application to superconducting metallic grains [98].

It is well-known that many-electron systems often possess several symmetries. For example, the Hubbard model [99] preserves total spin, total momentum, and some geometrical symmetries on a lattice. The fact that the Hubbard model cannot be solved analytically in arbitrary dimensions has led to intense research into numerical methods for these strongly correlated electron systems. It is crucially important to identify the symmetries and quantum numbers in understanding the nature of the ground state, where a symmetry breaking often occurs in the thermodynamic limit. Like in nuclei, the broken symmetry should be restored in finite size systems. Their excitation spectra and spectroscopic properties result from eigenstates of specified quantum numbers and play crucial roles in understanding the nature of low-energy phenomena in condensed matter physics.

Restoration of the spin symmetry was carried out [96] for the Hubbard model by considering a spin projection [100], which is the same technique as the angular–momentum-projection discussed in the present paper. Spin rotation is performed in the spin space and the spin projection is represented by one-dimensional integral of rotation. Quantum fluctuations were visualized in the 1D doped Hubbard model by using the spin projection [97].

In a more realistic calculation, a symmetry-projected configuration mixing scheme to describe ground and excited states, with well-defined quantum numbers, of the two-dimensional Hubbard model with nearest-neighbor hopping and periodic boundary conditions was presented in [101]. Despite of the above mentions applications, one realizes that while symmetry projected methods have been widely used for the nuclear physics problem, they have not been received sufficient attention in other fields such as condensed-matter physics and quantum chemistry. It was therefore suggested [102] that the symmetry-projection techniques deserve further consideration in the study of low-dimensional correlated many-electron systems.

7. Summary and perspective

To restore quantum numbers violated by spontaneous symmetry breakings in nuclei one applies the projection technique. Angular momentum projection is a known numerical method to recover the rotational symmetry which, as a conserved quantum number, lies at the foremost position in the discussion of nuclear many-body problems. The purpose of the present paper has been to emphasize, however, that our understanding of angular–momentum-projection may go beyond just a simple quantum-number restoration. Angular–momentum-projection method can be viewed as an efficient way of reorganizing, and more importantly, truncating the shell-model space. It transforms the states from the intrinsic system, where dominant excitation modes in the low-energy region are identified by applying the concept of spontaneous symmetry breaking, to the laboratory frame with physically well-defined configurations. Once in the angular–momentum-projected space, an energy-dictated, physically-guided shell-model truncation can be easily carried out. The projected bases are small in size but rich in physics, with which shell-model diagonalization will never pose a dimension problem and physical interpretation of the calculated results will become easy.

We have proven in section 3 that angular–momentum-projection emerges naturally if a deformed state is treated fully quantum-mechanically in the rotational space. The starting ansatz of the proof was the generalized wavefunction written as a superposition of all the rotated states in the spirit of GCM. The variational procedure led to eigenvalue equations expressed in the projected basis. We have shown that the generalized wavefunction, which is a superposition of (angular–momentum) projected states, becomes an eigenstate of angular momentum.

The above finding opens up possibilities to truncate the shell-model space. These possibilities do not exist in conventional shell models if one insists on the spherical basis. In section 5, we have shown several examples. If one is interested mainly in the yrast properties of a well-deformed nucleus with approximate axial symmetry, then the deformed basis does not need to be very sophisticated but a simple axially-deformed one. However, excited multi-qp configurations are important to be included in the projected basis. If the object nuclei either have an axially asymmetric shape or are soft without a well-defined shape, one should rather choose a deformed basis with triaxiality in deformation and perform three-dimensional angular–momentum-projection. As we have shown, such a basis is much more enriched and there are newly emerging states corresponding to experimental observations. On the other hand, an extended version containing additional phonon-like configurations in the projected basis gives possibilities to study the interplay between collective β-, γ-vibrations and qp excitations.

Technic details for the preparation of deformed qp basis, for evaluation of contractions and overlaps, for expression of rotated matrix elements, and for evaluation of projected matrix elements have been given in appendix. The presentation there has closely followed the original format in [21].

Before closing the present paper, we would like to mention two perspectives, one is technical and another is physical. The technical one is concerning the problem of how to compute efficiently the overlap of rotated matrix elements, which lies at the heart of the angular–momentum-projection theory. Although there is no problem in principle if one follows the pioneering works [103–105] for such calculation, one may encounter a practical problem of combinatorial complexity when more than 4-qp states are included in the basis configurations. The problem lies in the fact that the overlap matrix elements of multi-qp states are usually calculated with the generalized Wick's theorem [21], For example, as many as hundreds (thousands) terms are to be considered to express each matrix element with 4-qp (6-qp) state. Therefore, up to recently, 3-qp (4-qp) states have been allowed in the multi-qp configurations that can practically be treated in the PSM calculation, for odd-mass (even–even) systems [59, 106].

To push the calculation further toward extremes of angular momentum involving higher order of qp states, and to highly-excited energy regions where the nuclear astrophysics may find interest, a breakthrough in computational many-body techniques is needed. In nuclear structure physics, the Pfaffian concept has been introduced [107] as a key mathematical tool for solving the long-standing problem in the phase determination of the Onishi formula [108, 109]. Moreover, it has been shown that the Pfaffian algorithm is very efficient also for calculating overlap matrix elements [110–115]. In particular, by means of Fermion coherent states and Grassmann integral, an alternative approach to calculate the rotated matrix element for general qp states was derived [116], which serves as a theoretical framework to extend the PSM model space. In an initial attempt [117], the configuration space of the PSM has been expanded by using the Pfaffian method to include all kinds of 4-qp and some 6-qp states for both positive and negative parities. We expect that the Pfaffian method for many-body computation may be a new direction in the development of modern nuclear codes. We note that specific problems may be encountered when performing projection calculations, for example, in beyond-mean-field calculations when the energy density functional is not derived from a Hamiltonian operator [118–121].

As for the physical perspective, we should remark on the obvious limitation of the schematic interaction used in the present paper. In fact, the schematic forces may make sense only when they are used in conjunction with a single-particle Hamiltonian which binds nucleons tightly in space such as in the harmonic oscillator. Such a Hamiltonian does not allow nucleons to travel far away from the rest of the nucleus and is therefore inappropriate for the description of nuclei near the drip lines. One needs a more realistic Hamiltonian if some nucleons are loosely bound. Nevertheless, the framework of the present projection theory itself is still valid for more exotic systems.

For any nuclear structure calculations, the systematic description of nuclei along an isotopic or isotonic chain would fail if the empirical shell structure is not well reproduced. All this will naturally depend on details of the Hamiltonian and is therefore an important constraint on the Hamiltonian which may be used in nuclear structure problems. The 'good' results mentioned in the present paper rely heavily on phenomenological adjustments on the single-particle states obtained by, for example, the Nilsson model. Consequently, the model essentially provides no information about the unconventional shell evolution in neutron-rich nuclei where the single-particle structure is determined empirically. On the other hand, it has been known that the monopole interaction is a crucial ingredient for successful shell-model calculations [122]. The connection between the monopole interaction and the tensor force [123] was confirmed, which explains the shell evolution [124]. Recently, novel general properties of the monopole components in the effective interaction have been demonstrated by Otsuka *et al* [125] by introducing the monopole-based universal force, which consists of the Gaussian central force and the tensor force. This formalism was adopted in realistic shell-model calculations with the well-established pairing-plus-multipole force [126]. The so-constructed shell model was applied to a large number of nuclei in the *pf* and $pf_{5/2}g_{9/2}$ shell regions for both the near-ground-state region and high-spin excitations [126, 127]. It remains to be seen how such a monopole-based universal force can be combined into the Nilsson formalism which enables changes of the traditional single-particle field from 'static' to 'dynamic' along with the exotic shell evolution.

Acknowledgments

The initial projection idea is due largely to the late Dr K Hara, who inspired the present author when he studied at the Technical University of Munich in the 1980s. F-Q Chen, Z-C Gao, M W Guidry, J A Sheikh, L-J Wang, and C-L Wu have made important contributions in the different phases of the development of the theory. This work was supported by the National Natural Science Foundation of China (Nos. 11575112, 11135005), by the 973 Program of China (No. 2013CB834401), and by the Open Project Program of the State Key Laboratory of Theoretical Physics, Institute of Theoretical Physics, Chinese Academy of Sciences, China (No. Y5KF141CJ1).

Appendix A. Deformed quasiparticle basis

It is convenient to divide a numerical calculation with angular–momentum-projection into three main parts: preparation of the configuration space, calculation of the rotated matrix elements, and diagonalization in the projected basis. The following presentation closely follows the structure of the published computer codes for angular–momentum-projection [63] and the mathematical formulae given in [21].

Throughout the paper, we denote the annihilation operator in the spherical harmonic oscillator basis by $c_\alpha = c_{Njm}$ and its time-reversal by $c_{\bar\alpha} = \hat T c_\alpha \hat T^\dagger = (-)^{j-m} c_{Nj\,-m}$. It is noted that, under this phase convention and in the real representation, the time-reversal transformation $\hat T$ is equivalent to the unitary operator $\mathrm{e}^{-\imath\pi\hat J_y}$. Also, because of the identity

$$\mathrm{e}^{-\imath\pi\hat J_x} = \mathrm{e}^{-\imath\pi\hat J_y}\mathrm{e}^{-\imath\pi\hat J_z}, \tag{A1-1}$$

$\mathrm{e}^{-\imath\pi\hat J_x}$ and $\mathrm{e}^{-\imath\pi\hat J_z}$ do not represent mutually independent operations if the time-reversal is preserved. The former is the so-called signature operator. In our notation, we will use the latter to classify the basis states by defining a symmetry operator

$$\hat S = \mathrm{e}^{-\imath\pi\hat J_z}. \tag{A1-2}$$

This operator is convenient since it is diagonal in the spherical basis while the signature operator is not. The whole set of operators is thus classified into two classes according to

$$\hat S\, c_\alpha \hat S^\dagger = \mathrm{e}^{\imath m\pi} c_\alpha = \pm\imath c_\alpha, \tag{A1-3a}$$

$$\hat S\, c_{\bar\alpha}^\dagger \hat S^\dagger = \mathrm{e}^{\imath m\pi} c_{\bar\alpha}^\dagger = \pm\imath c_{\bar\alpha}^\dagger. \tag{A1-3b}$$

Here, the sign $+\,(-)$ applies to $m = \frac{1}{2}, -\frac{3}{2}, \frac{5}{2}, \ldots$ $\left(-\frac{1}{2}, \frac{3}{2}, -\frac{5}{2}, \ldots\right)$ and such a quantum number is denoted as $\alpha > 0$ ($\alpha < 0$) or referred to as of the class S ($\bar{\mathrm{S}}$). There is a one-to-one correspondence between the operators in the class S and $\bar{\mathrm{S}}$ which are related to each other through the time-reversal transformation. Note that, for a given quantum state α, the operators c_α and $c_{\bar\alpha}^\dagger$ belong to the same class whereas $c_{\bar\alpha}$ and $c_\alpha^\dagger$ to the other. The HFB transformation should be done within the same class of operators in order to preserve the symmetry described by (A1-2). For convenience, we will keep referring to the corresponding deformed single-particle basis denoted by a set of quantum number α as an 'Nilsson basis', no matter that they are created from a deformed Nilsson or Woods–Saxon potential, or from any other effective potentials. To be general, the following discussions will be made to cover not only the axially symmetric (spheroidal) deformation but also the triaxial (ellipsoidal) one.

The HFB qp operators which preserve the time-reversal invariance and have the symmetry described by $\hat S$ take the

form (in the real representation)

$$a_\nu = \sum_{\alpha>0}\{U_{\alpha\nu}c_\alpha + V_{\alpha\nu}c^\dagger_{\bar\alpha}\}, \tag{A1-4a}$$

$$a^\dagger_{\bar\nu} = \sum_{\alpha>0}\{-V_{\alpha\nu}c_\alpha + U_{\alpha\nu}c^\dagger_{\bar\alpha}\}, \tag{A1-4b}$$

where the summations run over the class S only. The qp operators (A1-4) then belong to the class S ($\nu > 0$). Those belonging to the class $\bar{\text{S}}$ ($\nu < 0$) can be obtained by applying the time-reversal transformation to (A1-4). The inverse of (A1-4) is given by

$$c_\alpha = \sum_{\nu>0}\{U_{\alpha\nu}a_\nu - V_{\alpha\nu}a^\dagger_{\bar\nu}\}, \tag{A1-5a}$$

$$c^\dagger_{\bar\alpha} = \sum_{\nu>0}\{V_{\alpha\nu}a_\nu + U_{\alpha\nu}a^\dagger_{\bar\nu}\}. \tag{A1-5b}$$

To summarize, in our convention, the HFB transformation is carried out among the operators belonging to the same class to ensure invariance with respect to the operator $\hat S$. Those belonging to different classes are mutually related with each other by the time-reversal transformation $\hat T$. The HFB vacuum state has the symmetry properties

$$\hat S|0\rangle = |0\rangle \quad \text{and} \quad \hat T|0\rangle = |0\rangle. \tag{A1-6}$$

These convenient properties avoid many common problems to happen in the numerical calculations with angular–momentum-projection. For example, in the phase determination of the Onishi formula [108] when the overlap of HFB wave functions is computed, there is sign problem for which special care needs to be taken [109,107].

Due to the unitarity of the HFB transformation, there is an identity $\sum_{\alpha>0}(c^\dagger_\alpha c_\alpha + c_{\bar\alpha}c^\dagger_{\bar\alpha}) = \sum_{\nu>0}(a^\dagger_\nu a_\nu + a_{\bar\nu}a^\dagger_{\bar\nu})$, which leads to

$$\sum_{\alpha>0}(c^\dagger_\alpha c_\alpha - c_{\bar\alpha}c^\dagger_{\bar\alpha}) = \sum_{\nu>0}(a^\dagger_\nu a_\nu - a_{\bar\nu}a^\dagger_{\bar\nu}) \equiv 2\hat M. \tag{A1-7}$$

It is an invariant operator which counts the difference between the number of particles or quasiparticles occupying the class S and $\bar{\text{S}}$ states. Since the HFB procedure inherently violates the conservation of the total number of particles

$$\hat N = \sum_{\alpha>0}(c^\dagger_\alpha c_\alpha + c^\dagger_{\bar\alpha}c_{\bar\alpha}), \tag{A1-8}$$

the operator $\hat M$ represents the 'next best' conserved quantity. It commutes with $\hat J_z$ but not with $\hat J_x$ or $\hat J_y$ and changes sign under the time-reversal transformation, $\hat T\hat M\hat T^\dagger = -\hat M$.

If, for simplicity, we define the qp basis by the Nilsson +BCS instead of the full HFB procedure, the HFB transformation amplitudes in (A1-4) become

$$U_{\alpha\nu} = W_{\alpha\nu}u_\nu \quad \text{and} \quad V_{\alpha\nu} = W_{\alpha\nu}v_\nu, \tag{A1-9}$$

where $W_{\alpha\nu}$ is the Nilsson amplitude and U_ν and v_ν the BCS amplitudes:

$$a_\nu = u_\nu b_\nu + v_\nu b^\dagger_{\bar\nu}, \quad b_\nu = \sum_{\alpha>0}W_{\alpha\nu}c_\alpha. \tag{A1-10}$$

The amplitudes $W_{\alpha\nu}$ in (A1-9) are obtained by diagonalizing the (ellipsoidal) Nilsson Hamiltonian for a given set of deformation parameters ε and ε'

$$\hat H_0 - \frac{3}{2}\hbar\omega\left\{\varepsilon\,\hat Q_0 + \varepsilon'\frac{\hat Q_{+2} + \hat Q_{-2}}{\sqrt{2}}\right\} \rightarrow \sum_{\nu>0}\varepsilon_\nu(b^\dagger_\nu b_\nu + b^\dagger_{\bar\nu}b_{\bar\nu}), \tag{A1-11}$$

where the operators $\hat H_0$ and $\hat Q_\mu$ are respectively defined by (23) and (24). For an axially symmetric system, we have $\varepsilon' = 0$.

In practice, we do not expect that the final results with angular–momentum-projection obtained in the Nilsson+BCS basis differ very much from those obtained in the HFB basis. This is because the final shell-model diagonalization can take into account properly the main effect of the coupling between the Quadrupole and Pairing force including the influence on the moment of inertia as well as on the coupling between the intrinsic (quasi-) particles and the rotating body. It is therefore possible to use the simpler Nilsson+BCS basis. As it is the deformed basis to start with the shell-model calculation, we do not need to make it more sophisticated than necessary in accordance with our basic philosophy.

It is convenient to write the relation (A1-5) in the matrix form

$$\text{Class S:}\quad \begin{bmatrix} c \\ c^\dagger \end{bmatrix} = \begin{bmatrix} U & -V \\ V & U \end{bmatrix}\begin{bmatrix} a \\ a^\dagger \end{bmatrix}. \tag{A1-12}$$

Note that this matrix relation holds among the operators of class S. For the operators of class $\bar{\text{S}}$, we have the relation

$$\text{Class } \bar{\text{S}}\text{:}\quad \begin{bmatrix} c \\ c^\dagger \end{bmatrix} = \begin{bmatrix} U & V \\ -V & U \end{bmatrix}\begin{bmatrix} a \\ a^\dagger \end{bmatrix} \tag{A1-13}$$

which follows from (A1-5a) by applying the time-reversal transformation $\hat T$. The relations $U_{\bar\alpha\bar\nu} = U_{\alpha\nu}$ and $V_{\bar\alpha\bar\nu} = V_{\alpha\nu}$ hold representing the time-reversal symmetry of the HFB transformation.

The rotation operator mixes the class S and $\bar{\text{S}}$. It is therefore convenient to write the above two relations in a 'large' form. With the definitions

$$U = \begin{bmatrix} U & 0 \\ 0 & U \end{bmatrix} \quad \text{and} \quad V = \begin{bmatrix} 0 & -V \\ V & 0 \end{bmatrix}. \tag{A1-14}$$

Equations (A1-12) and (A1-13) can be combined together as

$$\begin{bmatrix} c \\ c^\dagger \end{bmatrix} = \begin{bmatrix} U & V \\ V & U \end{bmatrix}\begin{bmatrix} a \\ a^\dagger \end{bmatrix}, \tag{A1-15}$$

where the operator arrays for particles and quasiparticles are arranged as $(c_\alpha, c_{\bar\alpha}, c^\dagger_\alpha, c^\dagger_{\bar\alpha})$ and $(a_\nu, a_{\bar\nu}, a^\dagger_\nu, a^\dagger_{\bar\nu})$, respectively. Since the transformation is unitary (with real matrix elements), the inverse of (A1-15) is given by

$$\begin{bmatrix} a \\ a^\dagger \end{bmatrix} = \begin{bmatrix} U & V \\ V & U \end{bmatrix}^t\begin{bmatrix} c \\ c^\dagger \end{bmatrix}, \tag{A1-16}$$

where t denotes the transpose of a matrix. The 'large' form is convenient for analytical derivations and the 'small' form for computer coding in numerical calculations. Decomposition of the former into the latter can be easily done by using (A1-14).

Appendix B. Evaluation of contractions and overlap

One of the basic ingredients of the angular–momentum-projection is the description of rotation of the deformed qp basis. It occurs in question because action of the angular–momentum-projector operator (11) on the ket state, when the matrix elements (18) are computed, involves a rotation operation of the deformed qp basis that defines the ket state. For the discussion purpose, we first note that the rotation of the spherical basis is attained on using the irreducible representation

$$\hat{R}(\Omega)c_\alpha\hat{R}^\dagger(\Omega)=\sum_{\alpha'}D_{\alpha\alpha'}(\Omega)c_{\alpha'}, \tag{A2-1}$$

where, explicitly, $D_{\alpha\alpha'}(\Omega)\equiv\delta_{NN'}\delta_{jj'}D^{j}_{mm'}(\Omega)$. The summation extends over all possible m', so that the rotation mixes two classes S and $\bar{\mathrm{S}}$. In the matrix form, one can write

$$\hat{R}(\Omega)\begin{bmatrix}c\\ c^\dagger\end{bmatrix}\hat{R}^\dagger(\Omega)=\begin{bmatrix}D(\Omega) & 0\\ 0 & D^*(\Omega)\end{bmatrix}\begin{bmatrix}c\\ c^\dagger\end{bmatrix}. \tag{A2-2}$$

It is sometimes convenient to decompose the 'large' matrix $D_{\alpha\alpha'}(\Omega)$ into the 'small' form by using the property $D_{\bar{\alpha}\bar{\alpha}'}(\Omega)=D^*_{\alpha\alpha'}(\Omega)$, and noting

$$D(\Omega)=\begin{bmatrix}D(\Omega) & \bar{D}(\Omega)\\ -\bar{D}^*(\Omega) & D^*(\Omega)\end{bmatrix}, \tag{A2-3}$$

where $\bar{D}_{\alpha\alpha'}(\Omega)\equiv D_{\alpha\bar{\alpha}'}(\Omega)=\delta_{NN'}\delta_{jj'}(-)^{j-m'}D^{j}_{m-m'}(\Omega)$.

Action of the rotation operator on the quasiparticles (A1-16) can be evaluated by using (A1-15) and (A2-2). The result is

$$\hat{R}(\Omega)\begin{bmatrix}a\\ a^\dagger\end{bmatrix}\hat{R}^\dagger(\Omega)=\begin{bmatrix}X(\Omega) & Y(\Omega)\\ Y^*(\Omega) & X^*(\Omega)\end{bmatrix}\begin{bmatrix}a\\ a^\dagger\end{bmatrix}, \tag{A2-4}$$

where

$$X(\Omega)=U^tD(\Omega)U+V^tD^*(\Omega)V, \tag{A2-5a}$$
$$Y(\Omega)=U^tD(\Omega)V+V^tD^*(\Omega)U. \tag{A2-5b}$$

The 'small' forms of these matrices can be obtained by using (A1-14) and (A2-3), i.e.

$$X(\Omega)=\begin{bmatrix}X(\Omega) & \bar{X}(\Omega)\\ -\bar{X}^*(\Omega) & X^*(\Omega)\end{bmatrix} \tag{A2-6a}$$

$$Y(\Omega)=\begin{bmatrix}\bar{Y}(\Omega) & -Y(\Omega)\\ Y^*(\Omega) & \bar{Y}^*(\Omega)\end{bmatrix}, \tag{A2-6b}$$

where

$$X(\Omega)=U^tD(\Omega)U+V^tD(\Omega)V, \tag{A2-7a}$$
$$\bar{X}(\Omega)=U^t\bar{D}(\Omega)U+V^t\bar{D}(\Omega)V, \tag{A2-7b}$$
$$Y(\Omega)=U^tD(\Omega)V-V^tD(\Omega)U, \tag{A2-7c}$$
$$\bar{Y}(\Omega)=U^t\bar{D}(\Omega)V-V^t\bar{D}(\Omega)U. \tag{A2-7d}$$

If the Nilsson+BCS basis is used instead of the HFB basis for calculations, the matrix elements in (A2-7) can be explicitly written as

$$X_{\nu\nu'}(\Omega)=x_{\nu\nu'}Z_{\nu\nu'}(\Omega),\quad \bar{X}_{\nu\nu'}(\Omega)=x_{\nu\nu'}\bar{Z}_{\nu\nu'}(\Omega), \tag{A2-8a}$$
$$Y_{\nu\nu'}(\Omega)=y_{\nu\nu'}Z_{\nu\nu'}(\Omega),\quad \bar{Y}_{\nu\nu'}(\Omega)=y_{\nu\nu'}\bar{Z}_{\nu\nu'}(\Omega), \tag{A2-8b}$$

where

$$x_{\nu\nu'}=u_\nu u_{\nu'}+v_\nu v_{\nu'},\quad y_{\nu\nu'}=u_\nu v_{\nu'}-v_\nu u_{\nu'} \tag{A2-9}$$

and

$$Z(\Omega)=W^tD(\Omega)W,\quad \bar{Z}(\Omega)=W^t\bar{D}(\Omega)W. \tag{A2-10}$$

To evaluate matrix elements expressed by creation and annihilation operators under rotation, we need to extend the usual Wick theorem and define three basic 'contractions'. Equation (A2-4) can be slightly rewritten as

$$\hat{R}(\Omega)a_\nu=\sum_\mu[X_{\nu\mu}(\Omega)a_\mu+Y_{\nu\mu}(\Omega)a^\dagger_\mu]\hat{R}(\Omega), \tag{A2-11a}$$

$$\hat{R}(\Omega)a^\dagger_\nu=\sum_\mu[Y^*_{\nu\mu}(\Omega)a_\mu+X^*_{\nu\mu}(\Omega)a^\dagger_\mu]\hat{R}(\Omega). \tag{A2-11b}$$

Taking the matrix element of the first equation of (A2-11) with respect to $\langle 0|$ and $a^\dagger_{\nu'}|0\rangle$, we can derive the relation (using the abbreviation $>\equiv|0\rangle$)

$$\langle a_\nu\hat{R}(\Omega)a^\dagger_{\nu'}\rangle=\langle\hat{R}(\Omega)\rangle[X^{-1}(\Omega)]_{\nu\nu'}. \tag{A2-12}$$

Similarly, on taking the matrix element with respect to $\langle 0|a_{\nu'}$ and $|0\rangle$, we derive

$$\langle a_\nu a_{\nu'}\hat{R}(\Omega)\rangle=\langle\hat{R}(\Omega)\rangle[X^{-1}(\Omega)Y(\Omega)]_{\nu\nu'}. \tag{A2-13}$$

Finally, we take the matrix element of the second equation of (A2-11) with respect to $\langle 0|$ and $a^\dagger_{\nu'}|0\rangle$ to derive

$$\langle\hat{R}(\Omega)a^\dagger_\nu a^\dagger_{\nu'}\rangle=\langle\hat{R}(\Omega)\rangle[Y^*(\Omega)X^{-1}(\Omega)]_{\nu\nu'}. \tag{A2-14}$$

If we introduce the operator

$$[\Omega]=\frac{\hat{R}(\Omega)}{\langle\hat{R}(\Omega)\rangle}, \tag{A2-15}$$

the above relations can be written as

$$C_{\nu\nu'}(\Omega)\equiv\langle a_\nu[\Omega]a^\dagger_{\nu'}\rangle=[X^{-1}(\Omega)]_{\nu\nu'} \tag{A2-16a}$$

$$B_{\nu\nu'}(\Omega)\equiv\langle a_\nu a_{\nu'}[\Omega]\rangle=[X^{-1}(\Omega)Y(\Omega)]_{\nu\nu'} \tag{A2-16b}$$

$$A_{\nu\nu'}(\Omega)\equiv\langle[\Omega]a^\dagger_\nu a^\dagger_{\nu'}\rangle=[Y^*(\Omega)X^{-1}(\Omega)]_{\nu\nu'}. \tag{A2-16c}$$

The operator (A2-15) is the three-dimensional form in space. It can be reduced to the one-dimensional operator

$$[\beta]=\frac{\mathrm{e}^{-\imath\beta\hat{J}_y}}{\langle\mathrm{e}^{-\imath\beta\hat{J}_y}\rangle} \tag{A2-17}$$

when dealing with an axially symmetric system.

Once the unitary coefficients $X(\Omega)$ and $Y(\Omega)$ are obtained, the 'contractions' $A(\Omega)$, $B(\Omega)$ and $C(\Omega)$ can be evaluated by

$$C(\Omega)=X^{-1}(\Omega)=\begin{bmatrix}C(\Omega) & \bar{C}(\Omega)\\ -\bar{C}^*(\Omega) & C^*(\Omega)\end{bmatrix}, \tag{A2-18a}$$

$$B(\Omega)=C(\Omega)Y(\Omega)=\begin{bmatrix}B(\Omega) & \bar{B}(\Omega)\\ -\bar{B}^*(\Omega) & B^*(\Omega)\end{bmatrix}, \tag{A2-18b}$$

$$A(\Omega)=Y^*(\Omega)C(\Omega)=\begin{bmatrix}A(\Omega) & \bar{A}(\Omega)\\ -\bar{A}^*(\Omega) & A^*(\Omega)\end{bmatrix}, \tag{A2-18c}$$

where the last forms of (A2-18) are their 'small' forms which can be expressed in terms of small matrices of $X(\Omega)$ and $Y(\Omega)$.

The remaining question is to evaluate the overlap $\langle\hat{R}(\Omega)\rangle$ appearing in equation (A2-15). The detailed derivation for it was given in [104, 105]. For the angular–momentum-projection but without particle number projection), $\langle\hat{R}(\Omega)\rangle$ is a real quantity

$$\langle\hat{R}(\Omega)\rangle = \{\det X(\Omega)\}^{\frac{1}{2}}. \tag{A2-19}$$

Moreover, using the small form (A2-6a) for $X(\Omega)$, we find that it is a positive quantity

$$\langle\hat{R}(\Omega)\rangle = |\det X(\Omega)|\{\det(1 + DD^*)\}^{\frac{1}{2}},$$
$$D \equiv X^{-1}(\Omega)\bar{X}(\Omega). \tag{A2-20}$$

It should be pointed out that the overlap will be a complex quantity for some other cases. For example, if $|0>$ is a Cranked HFB state, the quantity in equation (A2-19) is not real since the time-reversal is broken. In the case of a simultaneous angular momentum and particle number projection, it is not real either since the total operator is a sum of odd and even operator and has no definite time-reversal transformation property. The overlap is therefore a complex quantity in these examples. It means that, in such a case, the determinant of the matrix X is a complex quantity. Consequently, it is necessary to ensure that the right branch be selected when evaluating its square root numerically since the computer always takes the principal branch by convention, which is not necessarily the right one. If the wrong branch is picked at a mesh point, the integration (summation) over the group parameters may not be done properly since it leads to a subtraction instead of an addition.

Appendix C. Evaluation of rotated matrix elements

Using the contractions $A(\Omega)$, $B(\Omega)$ and $C(\Omega)$ obtained in (A2-16), it is easy to verify that the operator (A2-15) can be expressed in the form

$$[\Omega] = \exp\left\{-\frac{1}{2}\sum_{\nu\nu'} a_\nu^\dagger B_{\nu\nu'} a_{\nu'}^\dagger\right\} \exp\left\{\sum_{\nu\nu'} a_\nu^\dagger (\ln C)_{\nu\nu'} a_{\nu'}\right\} \times \exp\left\{-\frac{1}{2}\sum_{\nu\nu'} a_\nu A_{\nu\nu'} a_{\nu'}\right\}. \tag{A3-1}$$

Based on this relation, one can prove a generalized contraction theorem [104] which takes the form ($n + n'$= even with $m \equiv \max\left\{0, \frac{n-n'}{2}\right\}$)

$$\langle a_{n'}\cdots a_{1'}[\Omega]a_1^\dagger\cdots a_n^\dagger\rangle = \sum_{k=m}^{\left[\frac{n}{2}\right]}\sum_P (\pm)\,(B)^{k-(n-n')/2}(C)^{n-2k}(A)^k. \tag{A3-2}$$

Here, the right-hand side is a 'permuted sum' of products of $(n + n')/2$ contractions with all possible combinations of pairs of $n + n'$ indices and $(\pm)$ is the parity of the permutation. The type of the contraction between a pair of operators is A (B) if both of them stand on the right (left) side of $[\Omega]$ and is C if one of them stands on the left and the other on the right side of $[\Omega]$. The notation such as $(A)^k$ implies a product of k contractions of type A. This contraction rule can be intuitively understood by studying some examples. We give below those which involve four qp operators:

$$\langle a_1a_2a_3a_4[\Omega]\rangle = B_{12}(\Omega)B_{34}(\Omega) - B_{13}(\Omega)B_{24}(\Omega) + B_{14}(\Omega)B_{23}(\Omega), \tag{A3-3a}$$

$$\langle a_1a_2a_3[\Omega]a_4^\dagger\rangle = B_{12}(\Omega)C_{34}(\Omega) - B_{13}(\Omega)C_{24}(\Omega) + C_{14}(\Omega)B_{23}(\Omega), \tag{A3-3b}$$

$$\langle a_1a_2[\Omega]a_3^\dagger a_4^\dagger\rangle = B_{12}(\Omega)A_{34}(\Omega) - C_{13}(\Omega)C_{24}(\Omega) + C_{14}(\Omega)C_{23}(\Omega), \tag{A3-3c}$$

$$\langle a_1[\Omega]a_2^\dagger a_3^\dagger a_4^\dagger\rangle = C_{12}(\Omega)A_{34}(\Omega) - C_{13}(\Omega)A_{24}(\Omega) + C_{14}(\Omega)A_{23}(\Omega), \tag{A3-3d}$$

$$\langle[\Omega]a_1^\dagger a_2^\dagger a_3^\dagger a_4^\dagger\rangle = A_{12}(\Omega)A_{34}(\Omega) - A_{13}(\Omega)A_{24}(\Omega), + A_{14}(\Omega)A_{23}(\Omega). \tag{A3-3e}$$

Thus, the evaluation of the 'rotated' matrix element can be made by first writing

$$\langle a_{n'}\ldots a_{1'}\hat{R}(\Omega)a_1^\dagger\ldots a_n^\dagger\rangle = \langle\hat{R}(\Omega)\rangle\langle a_{n'}\ldots a_{1'}[\Omega]\,a_1^\dagger\ldots a_n^\dagger\rangle \tag{A3-4}$$

and then expressing the right-hand side in terms of overlap (A2-19) and contractions (A2-18) with the help of the rule (A3-2).

As an example, let us consider a one-body operator $\hat{O}$. There are four kinds of 'basic' contractions, namely

$$\langle\hat{O}[\Omega]\rangle,\ \langle\hat{O}[\Omega]a_1^\dagger a_2^\dagger\rangle,\ \langle a_1\hat{O}[\Omega]a_2^\dagger\rangle,\ \langle a_1a_2\hat{O}[\Omega]\rangle. \tag{A3-5}$$

We can express any (higher order) contractions of $\hat{O}$ in terms of these basic ones. It will be convenient to write them in the form

$$\langle\hat{O}[\Omega]a_1^\dagger a_2^\dagger\rangle = \langle\hat{O}[\Omega]\rangle\langle[\Omega]a_1^\dagger a_2^\dagger\rangle + (\hat{O}[\Omega]a_1^\dagger a_2^\dagger), \tag{A3-6a}$$

$$\langle a_1\hat{O}[\Omega]a_2^\dagger\rangle = \langle\hat{O}[\Omega]\rangle\langle a_1[\Omega]a_2^\dagger\rangle + (a_1\hat{O}[\Omega]a_2^\dagger), \tag{A3-6b}$$

$$\langle\hat{a}_1a_2O[\Omega]\rangle = \langle\hat{O}[\Omega]\rangle\langle a_1a_2[\Omega]\rangle + (a_1a_2\hat{O}[\Omega]). \tag{A3-6c}$$

The symbol $(\cdots[\Omega]\cdots)$ will be referred to as 'linked' contraction, which implies that contractions between external indices (quantum numbers 1 and 2) should not be taken. Linked contractions will vanish identically when external

indices are contracted:

$$([\Omega]a_1^\dagger a_2^\dagger) = (a_1[\Omega]a_2^\dagger) = (a_1a_2[\Omega]) = 0. \tag{A3-7}$$

In fact, since $\langle[\Omega]\rangle = 1$, the above properties follow from (A3-6) by taking $\hat{O} = 1$. The vacuum contraction $(\hat{O}[\Omega])$ is identical to $\langle\hat{O}[\Omega]\rangle$ as there is no external index. Below, we present formulas for the linked contractions of a general one-body operator $\hat{O}$ which we separate into a c-number part and an operator part as $\hat{O} = <\hat{O}> + :\hat{O}:$

$$:\hat{O}: = \sum_{\nu\nu'}\left\{a_\nu^\dagger O^{(1)}_{\nu\nu'}a_{\nu'} + \frac{1}{2}[a_\nu^\dagger O^{(2)}_{\nu\nu'}a_{\nu'}^\dagger - a_\nu O^{(3)}_{\nu\nu'}a_{\nu'}]\right\}. \tag{A3-8}$$

Matrices $O^{(2)}$ and $O^{(3)}$ are anti-symmetric. If $\hat{O}$ is a Hermitian operator, then $O^{(1)}$ is Hermitian and $O^{(3)} = O^{(2)}*$. In practice, we may assume that they are real matrices.

The linked contractions of $:\hat{O}:$ become

$$\langle:\hat{O}:[\Omega]\rangle = -\frac{1}{2}\mathrm{Tr}\{O^{(B3)}\}, \tag{A3-9a}$$

$$(a_1:\hat{O}:[\Omega]\,a_2^\dagger) = O^{(1C)}_{12} + O^{(B3C)}_{12} \tag{A3-9b}$$

$$(:\hat{O}:[\Omega]\,a_1^\dagger a_2^\dagger) = O^{(C3C)}_{12}, \tag{A3-9c}$$

$$(a_2a_1:\hat{O}:[\Omega]) = O^{(2)}_{12} - O^{(1B)}_{12} - O^{(B3B)}_{12}, \tag{A3-9d}$$

where the following matrices are introduced

$$O^{(1B)} = O^{(1)}B(\Omega) - B^t(\Omega)O^{(1)t}, \tag{A3-10a}$$

$$O^{(1C)} = O^{(1)}C(\Omega), \tag{A3-10b}$$

$$O^{(B3)} = B^t(\Omega)O^{(3)}, \tag{A3-10c}$$

$$O^{(B3B)} = O^{(B3)}B(\Omega), \tag{A3-10d}$$

$$O^{(B3C)} = O^{(B3)}C(\Omega), \tag{A3-10e}$$

$$O^{(C3C)} = C^t(\Omega)O^{(3)}C(\Omega). \tag{A3-10f}$$

Similarly, for the operator

$$:\hat{O}^\dagger: = \sum_{\nu\nu'}\left\{a_\nu^\dagger O^{(1)t}_{\nu\nu'}a_{\nu'} + \frac{1}{2}[a_\nu^\dagger O^{(3)}_{\nu\nu'}a_{\nu'}^\dagger - a_\nu O^{(2)}_{\nu\nu'}a_{\nu'}]\right\}, \tag{A3-11}$$

we obtain

$$\langle:\hat{O}^\dagger:[\Omega]\rangle = -\frac{1}{2}\mathrm{Tr}\{O^{(B2)}\}, \tag{A3-12a}$$

$$(a_1:\hat{O}^\dagger:[\Omega]\,a_2^\dagger) = O^{(0C)}_{12} + O^{(B2C)}_{12}, \tag{A3-12b}$$

$$(:\hat{O}^\dagger:[\Omega]\,a_1^\dagger a_2^\dagger) = O^{(C2C)}_{12}, \tag{A3-12c}$$

$$(a_2a_1:\hat{O}^\dagger:[\Omega]) = O^{(3)}_{12} - O^{(0B)}_{12} - O^{(B2B)}_{12}, \tag{A3-12d}$$

where

$$O^{(0B)} = O^{(1)t}B(\Omega) - B^t(\Omega)O^{(1)}, \tag{A3-13a}$$

$$O^{(0C)} = O^{(1)t}C(\Omega), \tag{A3-13b}$$

$$O^{(B2)} = B^t(\Omega)O^{(2)}, \tag{A3-13c}$$

$$O^{(B2B)} = O^{(B2)}B(\Omega), \tag{A3-13d}$$

$$O^{(B2C)} = O^{(B2)}C(\Omega), \tag{A3-13e}$$

$$O^{(C2C)} = C^t(\Omega)O^{(2)}C(\Omega). \tag{A3-13f}$$

These formulas are of much practical importance. Since the two-body interaction of the present model is a sum of separable forces, the direct matrix elements can be expressed in terms of the quantities such as (A3-9) and (A3-12). This will save much memory and computing time and is one of the advantages of the present model. On the other hand, the exchange matrix elements of separable forces are less important due to the absence of the coherence (which has been confirmed numerically in an earlier work [105]) and will be neglected in accordance with the usual treatment of separable forces.

Let us consider a Hermitian two-body operator representing a separable force

$$\begin{aligned}\hat{H} = \hat{O}^\dagger\hat{O} &= \langle\hat{O}\rangle^2 + \langle\hat{O}\rangle\{:\hat{O}^\dagger: + :\hat{O}:\} + :\hat{O}^\dagger::\hat{O}: \\ &\equiv H^{(0)} + \hat{H}^{(1)} + \hat{H}^{(2)}\end{aligned} \tag{A3-14}$$

where $H^{(0)}$ is a c-number and $\hat{H}^{(1)}$ ($\hat{H}^{(2)}$) is that part which contains 2 (4) qp operators. Evaluation of $\hat{H}^{(1)}$ proceeds in the same way as for the one-body operator, namely its vacuum contraction is given by

$$\langle H^{(1)}[\Omega]\rangle = \langle\hat{O}\rangle\{\langle:\hat{O}^\dagger:[\Omega]\rangle + \langle:\hat{O}:[\Omega]\rangle\} \tag{A3-15}$$

while linked contractions become

$$\begin{aligned}(\hat{H}^{(1)}[\Omega]a_1^\dagger a_2^\dagger) &= \langle\hat{O}\rangle\{(:\hat{O}^\dagger:[\Omega]a_1^\dagger a_2^\dagger) + (:\hat{O}:[\Omega]a_1^\dagger a_2^\dagger)\}, \\ (a_1\hat{H}^{(1)}[\Omega]a_2^\dagger) &= \langle\hat{O}\rangle\{(a_1:\hat{O}^\dagger:[\Omega]a_2^\dagger) + (a_1:\hat{O}:[\Omega]a_2^\dagger)\}, \\ (a_2a_1\hat{H}^{(1)}[\Omega]) &= \langle\hat{O}\rangle\{(a_2a_1:\hat{O}^\dagger:[\Omega]) + (a_2a_1:\hat{O}:[\Omega])\}.\end{aligned} \tag{A3-16}$$

The treatment of $\hat{H}^{(2)}$ is more complex. First, the vacuum contraction is given by

$$\langle H^{(2)}[\Omega]\rangle = \langle:\hat{O}^\dagger:[\Omega]\rangle\langle:\hat{O}:[\Omega]\rangle. \tag{A3-17}$$

There are eight possible linked contractions for $\hat{H}^{(2)}$. The first three are 2-qp type which are similar to those of $\hat{H}^{(1)}$ (and may be combined with (A3-16)):

$$\begin{aligned}(\hat{H}^{(2)}[\Omega]a_1^\dagger a_2^\dagger) &= \langle:\hat{O}^\dagger:[\Omega]\rangle(:\hat{O}:[\Omega]a_1^\dagger a_2^\dagger) \\ &\quad + \langle:\hat{O}:[\Omega]\rangle(:\hat{O}^\dagger:[\Omega]a_1^\dagger a_2^\dagger),\end{aligned} \tag{A3-18a}$$

$$\begin{aligned}(a_1\hat{H}^{(2)}[\Omega]a_2^\dagger) &= \langle:\hat{O}^\dagger:[\Omega]\rangle(a_1:\hat{O}:[\Omega]a_2^\dagger) \\ &\quad + \langle:\hat{O}:[\Omega]\rangle(a_1:\hat{O}^\dagger:[\Omega]a_2^\dagger),\end{aligned} \tag{A3-18b}$$

$$\begin{aligned}(a_2a_1\hat{H}^{(2)}[\Omega]) &= \langle:\hat{O}^\dagger:[\Omega]\rangle(a_2a_1:\hat{O}:[\Omega]) \\ &\quad + \langle:\hat{O}:[\Omega]\rangle(a_2a_1:\hat{O}^\dagger:[\Omega]).\end{aligned} \tag{A3-18c}$$

The remaining five are of the 4-qp type:

$$(\hat{H}^{(2)}[\Omega]a_1^\dagger a_2^\dagger a_3^\dagger a_4^\dagger) = (:\hat{O}^\dagger:[\Omega]a_1^\dagger a_2^\dagger)(:\hat{O}:[\Omega]a_3^\dagger a_4^\dagger)$$
$$+ (:\hat{O}:[\Omega]a_1^\dagger a_2^\dagger)(:\hat{O}^\dagger:[\Omega]a_3^\dagger a_4^\dagger)$$
$$- (:\hat{O}^\dagger:[\Omega]a_1^\dagger a_3^\dagger)(:\hat{O}:[\Omega]a_2^\dagger a_4^\dagger)$$
$$- (:\hat{O}:[\Omega]a_1^\dagger a_3^\dagger)(:\hat{O}^\dagger:[\Omega]a_2^\dagger a_4^\dagger)$$
$$+ (:\hat{O}^\dagger:[\Omega]a_1^\dagger a_4^\dagger)(:\hat{O}:[\Omega]a_2^\dagger a_3^\dagger)$$
$$+ (:\hat{O}:[\Omega]a_1^\dagger a_4^\dagger)(:\hat{O}^\dagger:[\Omega]a_2^\dagger a_3^\dagger), \tag{A3-19}$$

$$(a_1\hat{H}^{(2)}[\Omega]a_2^\dagger a_3^\dagger a_4^\dagger) = (a_1:\hat{O}^\dagger:[\Omega]a_2^\dagger)(:\hat{O}:[\Omega]a_3^\dagger a_4^\dagger)$$
$$+ (a_1:\hat{O}:[\Omega]a_2^\dagger)(:\hat{O}^\dagger:[\Omega]a_3^\dagger a_4^\dagger)$$
$$- (a_1:\hat{O}^\dagger:[\Omega]a_3^\dagger)(:\hat{O}:[\Omega]a_2^\dagger a_4^\dagger)$$
$$- (a_1:\hat{O}:[\Omega]a_3^\dagger)(:\hat{O}^\dagger:[\Omega]a_2^\dagger a_4^\dagger)$$
$$+ (a_1:\hat{O}^\dagger:[\Omega]a_4^\dagger)(:\hat{O}:[\Omega]a_2^\dagger a_3^\dagger)$$
$$+ (a_1:\hat{O}:[\Omega]a_4^\dagger)(:\hat{O}^\dagger:[\Omega]a_2^\dagger a_3^\dagger), \tag{A3-20}$$

$$(a_2a_1\hat{H}^{(2)}[\Omega]a_3^\dagger a_4^\dagger) = (a_2a_1:\hat{O}^\dagger:[\Omega])(:\hat{O}:[\Omega]a_3^\dagger a_4^\dagger)$$
$$+ (a_2a_1:\hat{O}:[\Omega])(:\hat{O}^\dagger:[\Omega]a_3^\dagger a_4^\dagger)$$
$$- (a_2:\hat{O}^\dagger:[\Omega]a_3^\dagger)(a_1:\hat{O}:[\Omega]a_4^\dagger)$$
$$- (a_2:\hat{O}:[\Omega]a_3^\dagger)(a_1:\hat{O}^\dagger:[\Omega]a_4^\dagger)$$
$$+ (a_2:\hat{O}^\dagger:[\Omega]a_4^\dagger)(a_1:\hat{O}:[\Omega]a_3^\dagger)$$
$$+ (a_2:\hat{O}:[\Omega]a_4^\dagger)(a_1:\hat{O}^\dagger:[\Omega]a_3^\dagger), \tag{A3-21}$$

$$(a_3a_2a_1\hat{H}^{(2)}[\Omega]a_4^\dagger) = (a_2a_1:\hat{O}^\dagger:[\Omega])(a_3:\hat{O}:[\Omega]a_4^\dagger)$$
$$+ (a_2a_1:\hat{O}:[\Omega])(a_3:\hat{O}^\dagger:[\Omega]a_4^\dagger)$$
$$- (a_3a_1:\hat{O}^\dagger:[\Omega])(a_2:\hat{O}:[\Omega]a_4^\dagger)$$
$$- (a_3a_1:\hat{O}:[\Omega])(a_2:\hat{O}^\dagger:[\Omega]a_4^\dagger)$$
$$+ (a_1:\hat{O}^\dagger:[\Omega]a_4^\dagger)(a_3a_2:\hat{O}:[\Omega])$$
$$+ (a_1:\hat{O}:[\Omega]a_4^\dagger)(a_3a_2:\hat{O}^\dagger:[\Omega]), \tag{A3-22}$$

$$(a_4a_3a_2a_1\hat{H}^{(2)}[\Omega]) = (a_2a_1:\hat{O}^\dagger:[\Omega])(a_4a_3:\hat{O}:[\Omega])$$
$$+ (a_2a_1:\hat{O}:[\Omega])(a_4a_3:\hat{O}^\dagger:[\Omega])$$
$$- (a_3a_1:\hat{O}^\dagger:[\Omega])(a_4a_2:\hat{O}:[\Omega])$$
$$- (a_3a_1:\hat{O}:[\Omega])(a_4a_2:\hat{O}^\dagger:[\Omega])$$
$$+ (a_4a_1:\hat{O}^\dagger:[\Omega])(a_3a_2:\hat{O}:[\Omega])$$
$$+ (a_4a_1:\hat{O}:[\Omega])(a_3a_2:\hat{O}^\dagger:[\Omega]). \tag{A3-23}$$

Note that, in evaluating the contractions of $\hat{H}^{(2)}$, only those terms which factorize to two one-body contractions are retained since they are the terms which benefit from the maximal coherence. They represent the direct type matrix elements. All other matrix elements are neglected since they are of exchange types.

Let us now consider the matrix elements of the operators $\hat{H}^{(1)}$ and $\hat{H}^{(2)}$ in (A3-14) between two multi-qp states

$$|\Phi\{n\}\rangle = a_1^\dagger \ldots a_n^\dagger|0\rangle \quad \text{and} \quad |\Phi\{n'\}\rangle = a_1^\dagger \ldots a_{n'}^\dagger|0\rangle, \tag{A3-24}$$

where the sum of the number of quasiparticles in these states $(n + n')$ has to be an even number. We obtain for the operator $\hat{H}^{(1)}$:

$$\langle\Phi\{n'\}|\hat{H}^{(1)}[\Omega]|\Phi\{n\}\rangle = \langle\hat{H}^{(1)}[\Omega]\rangle\langle\Phi\{n'\}|[\Omega]|\Phi\{n\}\rangle$$
$$+ \sum(\pm)(\hat{H}^{(1)}[\Omega]a_i^\dagger a_j^\dagger)\langle\Phi\{n'\}|[\Omega]|\Phi\{n;\,i,j\}\rangle$$
$$+ \sum(\pm)(a_{i'}\hat{H}^{(1)}[\Omega]a_i^\dagger)\langle\Phi\{n';\,j'\}|[\Omega]|\Phi\{n;\,i\}\rangle$$
$$+ \sum(\pm)(a_{j'}a_{i'}\hat{H}^{(1)}[\Omega])\langle\Phi\{n';\,i',j'\}|[\Omega]|\Phi\{n\}\rangle, \tag{A3-25}$$

where $|\Phi\{n;\,i,j\}\rangle$ etc means a state which is obtained by removing the quasiparticles $a_i^\dagger$ and $a_j^\dagger$ from the state $|\Phi\{n\}\rangle$. Similarly, we obtain for the operator $\hat{H}^{(2)}$:

$$\langle\Phi\{n'\}|\hat{H}^{(2)}[\Omega]|\Phi\{n\}\rangle = \langle\hat{H}^{(2)}[\Omega]\rangle\langle\Phi\{n'\}|[\Omega]|\Phi\{n\}\rangle$$
$$+ \sum(\pm)(\hat{H}^{(2)}[\Omega]a_i^\dagger a_j^\dagger)\langle\Phi\{n'\}|[\Omega]|\Phi\{n;\,i,j\}\rangle$$
$$+ \sum(\pm)(a_{i'}\hat{H}^{(2)}[\Omega]a_i^\dagger)\langle\Phi\{n';\,i'\}|[\Omega]|\Phi\{n;\,i\}\rangle$$
$$+ \sum(\pm)(a_{j'}a_{i'}\hat{H}^{(2)}[\Omega])\langle\Phi\{n';\,i',j'\}|[\Omega]|\Phi\{n\}\rangle$$
$$+ \sum(\pm)(\hat{H}^{(2)}[\Omega]a_i^\dagger a_j^\dagger a_k^\dagger a_l^\dagger)$$
$$\times\langle\Phi\{n'\}|[\Omega]|\Phi\{n;\,i,j,k,l\}\rangle$$
$$+ \sum(\pm)(a_{i'}\hat{H}^{(2)}[\Omega]a_i^\dagger a_j^\dagger a_k^\dagger)$$
$$\times\langle\Phi\{n';\,i'\}|[\Omega]|\Phi\{n;\,i,j,k\}\rangle$$
$$+ \sum(\pm)(a_{j'}a_{i'}\hat{H}^{(2)}[\Omega]a_i^\dagger a_j^\dagger)$$
$$\times\langle\Phi\{n';\,i',j'\}|[\Omega]|\Phi\{n;\,i,j\}\rangle$$
$$+ \sum(\pm)(a_{k'}a_{j'}a_{i'}\hat{H}^{(2)}[\Omega]a_i^\dagger)$$
$$\times\langle\Phi\{n';\,i',j',k'\}|[\Omega]|\Phi\{n;\,i\}\rangle$$
$$+ \sum(\pm)(a_{l'}a_{k'}a_{j'}a_{i'}\hat{H}^{(2)}[\Omega])$$
$$\times\langle\Phi\{n';\,i',j',k',l'\}|[\Omega]|\Phi\{n\}\rangle. \tag{A3-26}$$

The summations are over permutations. The contractions appearing in these formulas can be evaluated by using (A3-15) –(A3-23) and overlaps of two states by (A3-2).

Appendix D. Evaluation of projected matrix elements and solution of the eigenvalue equation

The last step is the integration over the group parameters. The projected matrix element between two intrinsic states in general takes the form

$$\langle\Phi\{n'\}|\hat{P}^{I'}_{K'M'}\hat{T}_{\lambda\mu}\hat{P}^{I}_{KM}|\Phi\{n\}\rangle = (IM,\,\lambda\mu|I'M')$$
$$\times\sum_\nu(IK'-\nu,\,\lambda\nu|I'K')$$
$$\times\langle\Phi\{n'\}|\hat{T}_{\lambda\nu}\hat{P}^{I}_{K'-\nu K}|\Phi\{n\}\rangle. \tag{A4-1}$$

The operator $\hat{T}_{\lambda\mu}$ was originally considered to be a one-body (multipole) operator but the formula is actually valid for any spherical tensor operators. For example, we could also take it to be 1 (norm) or $\hat{H}$ (Hamiltonian) in which case we have $\lambda = \mu = 0$. In what follows, we will thus examine the three-fold integration in the projected matrix element (using the abbreviations $|\Phi\rangle \equiv |\Phi\{n\}\rangle$ and $|\Phi'\rangle \equiv |\Phi\{n'\}\rangle$):

$$\langle\Phi'|\hat{T}_{\lambda\nu}\hat{P}^{I}_{K'-\nu K}|\Phi\rangle = \frac{2I+1}{8\pi^2}\int \mathrm{d}\Omega\, D^{I}_{K'-\nu K}(\Omega)\langle\Phi'|\hat{T}_{\lambda\nu}\hat{R}(\Omega)|\Phi\rangle. \quad \text{(A4-2)}$$

In order to accelerate the computation, it is essential to use an efficient algorithm to evaluate the rotated matrix element $\langle\Phi'|\hat{T}_{\lambda\nu}\hat{R}(\Omega)|\Phi\rangle$ since it has to be computed at each mesh point of Ω for all possible qp configurations taken into account. This aspect was discussed in the previous section. Moreover, the same rotated matrix element is used to compute the projected matrix elements for different spins (i.e. the dependence on I, K and K' comes only from the D-function) so that we can take the advantage of this feature to speed up the computation. Another important strategy is to reduce the range of the integrations (i.e. the number of mesh points of Ω) by using the symmetry properties of the integrand. Such a consideration is especially important when carrying out a triaxial projection (three-fold integration over complex functions) which can be quite time-consuming.

The integrations in (A4-2) are evaluated by using appropriate quadrutures (e.g. the Gauß–Legendre for β- and trapezoidal formulas for α- and γ-integration). They are the standard problems of the numerical analysis and will not be discussed.

When a new code for angular–momentum-projection is written, one might wish to test it before applying to actual problems. In particular, the test of that part that is related to the PSM eigenvalue equation will be essential among other parts of the programme. In this sense, the most important quantities are the Hamiltonian and norm matrix elements

$$H^{I}_{\kappa K\,\kappa' K'} = \langle\Phi_\kappa|\hat{H}\hat{P}^{IN}_{KK'}|\Phi_{\kappa'}\rangle, \quad \text{(A4-3a)}$$

$$N^{I}_{\kappa K\,\kappa' K'} = \langle\Phi_\kappa|\hat{P}^{IN}_{KK'}|\Phi_{\kappa'}\rangle, \quad \text{(A4-3b)}$$

which constitute the basic ingredients of the PSM eigenvalue equation.

To test the coding and check the numerical accuracy, two sum rules

$$\sum_{IM} H^{I}_{\kappa M\,\kappa' M} = \langle\Phi_\kappa|\hat{H}\hat{P}^{N}|\Phi_{\kappa'}\rangle, \quad \text{(A4-4a)}$$

$$\sum_{IM} N^{I}_{\kappa M\,\kappa' M} = \langle\Phi_\kappa|\hat{P}^{N}|\Phi_{\kappa'}\rangle \quad \text{(A4-4b)}$$

are most useful. Make the replacements $\hat{P}^{IN}_{KK'} \to \hat{P}^{I}_{KK'}$ and $\hat{P}^{N} \to 1$ if the particle number projection is to be omitted. The summation over I may be terminated at a sufficiently large value since the magnitudes of the projected matrix elements decrease rapidly beyond a certain value of I.

For an axially symmetric system, the Hamiltonian and norm elements are written as

$$H^{I}_{\kappa\kappa'} = \langle\Phi_\kappa|\hat{H}\hat{P}^{IN}_{KK'}|\Phi_{\kappa'}\rangle \quad \text{and} \quad N^{I}_{\kappa\kappa'} = \langle\Phi_\kappa|\hat{P}^{IN}_{KK'}|\Phi_{\kappa'}\rangle, \quad \text{(A4-5)}$$

where K and K' are respectively the conserved (intrinsic) K-quantum number of $|\Phi_\kappa\rangle$ and $|\Phi_{\kappa'}\rangle$, so that the summation over M reduces to a single term with $M = K = K'$. If the particle number projection is omitted, for example, the sum rules become

$$\sum_I H^{I}_{\kappa\kappa'} = \langle\Phi_\kappa|\hat{H}|\Phi_{\kappa'}\rangle \quad \text{and} \quad \sum_I N^{I}_{\kappa\kappa'} = \langle\Phi_\kappa|\Phi_{\kappa'}\rangle. \quad \text{(A4-6)}$$

Note that both sides vanish if $K \neq K'$. It means unfortunately that nontrivial sum rules exist only for the matrix elements of $K = K'$ in the axially symmetric case.

Let us now turn to the discussion of how to solve the eigenvalue equation

$$\sum_{\kappa' K'}\{H^{I}_{\kappa K\,\kappa' K'} - E N^{I}_{\kappa K\,\kappa' K'}\}F^{I}_{\kappa' K'} = 0. \quad \text{(A4-7)}$$

We introduce and work in the representation in which the norm matrix is diagonal

$$\sum_{\kappa' K'} N^{I}_{\kappa K\,\kappa' K'} U^{\sigma}_{\kappa' K'} = n_\sigma U^{\sigma}_{\kappa K}. \quad \text{(A4-8)}$$

The norm eigenvalues n_σ are nonnegative quantities since the norm is a positive semi-definite matrix. However, it is quite possible that some of them vanish. This happens under the circumstances that the multi-qp states become linearly dependent when they are projected. It implies that the PSM basis contains some redundant states. Such redundant states can be removed simply by discarding the zero-eigenvalue solutions of (A4-8) since the norm (length) of such a state becomes zero. In fact, we find that $\langle U^{\sigma}|U^{\sigma}\rangle = n_\sigma$, namely $|U^{\sigma}\rangle \equiv \sum_{\kappa K} U^{\sigma}_{\kappa K}\hat{P}^{IN}_{MK}|\Phi_\kappa\rangle = 0$ if $n_\sigma = 0$, which implies nothing other than the linear dependence of the projected multi-qp states. We may exclude all solutions of (A4-8) corresponding to $n_\sigma = 0$ since $|U^{\sigma}\rangle$ vanishes.

In the basis of $\{|U^{\sigma}\rangle, n_\sigma \neq 0\}$, the PSM eigenvalue equation takes the form

$$\sum_{\sigma'} G^{I}_{\sigma\sigma'} V^{E}_{\sigma'} = E\, V^{E}_{\sigma}, \quad \text{(A4-9a)}$$

$$G^{I}_{\sigma\sigma'} = \frac{\sum_{\kappa K\kappa' K'} U^{\sigma}_{\kappa K} H^{I}_{\kappa K\,\kappa' K'} U^{\sigma'}_{\kappa' K'}}{\sqrt{n_\sigma n_{\sigma'}}} \quad \text{(A4-9b)}$$

from which the eigenvaector V^{E}_{σ} and the energy E are obtained. In the original muti-qp basis, the PSM amplitude corresponding to the energy E takes the (nonunitary) form

$$F^{I}_{\kappa K} = \sum_\sigma \frac{V^{E}_{\sigma} U^{\sigma}_{\kappa K}}{\sqrt{n_\sigma}} \quad \text{(A4-10)}$$

which satisfies automatically the normalization condition (40)

$$\sum_{\kappa K\kappa' K'} F^{I}_{\kappa K} N^{I}_{\kappa K\kappa' K'} F^{I}_{\kappa' K'} = 1, \quad \text{(A4-11)}$$

provided that the eigenvectors of (A4-8) and (A4-9) are normalized to unity. For axially symmetric systems, we

remove all summations over the K-quantum numbers and omit K in the amplitude $F^{I}_{\kappa K}$ as described previously.

References

[1] Caurier E, Martinez-Pinedo G, Nowacki F, Poves A and Zuker A P 2005 *Rev. Mod. Phys.* **77** 427
[2] Ring P and Schuck P 1980 *The Nuclear Many-Body Problem* (New York: Spring)
[3] Bohr A and Mottelson B R 1998 *Nuclear Structure* (Singapore: World Scientific)
[4] de Voigt M J A, Dudek J and Szymański Z 1983 *Rev. Mod. Phys.* **55** 949
[5] Frauendorf S 2001 *Rev. Mod. Phys.* **73** 463
[6] Hara K, Hayashi A and Ring P 1982 *Nucl. Phys.* A **385** 14
[7] Hayashi A, Hara K and Ring P 1984 *Phys. Rev. Lett.* **53** 337
[8] Kamlah A 1968 *Z. Phys.* **216** 52
[9] Enami K, Tanabe K and Yoshinaga N 1999 *Phys. Rev.* C **59** 135
[10] Enami K, Tanabe K and Yoshinaga N 2000 *Phys. Rev.* C **61** 027301
[11] Egido J L, Robledo L M and Sun Y 1993 *Nucl. Phys.* A **560** 253
[12] Sun Y, Robledo L M and Egido J L 1994 *Nucl. Phys.* A **570** 305c
[13] Rodriguez T R and Egido J L 2010 *Phys. Rev.* C **81** 064323
[14] Rodriguez T R and Egido J L 2011 *Phys. Lett.* B **705** 255
[15] Yao J M, Bender M and Heenen P-H 2013 *Phys. Rev.* C **87** 034322
[16] Fu Y *et al* 2013 *Phys. Rev.* C **87** 054305
[17] Zuker A P, Retamosa J, Poves A and Caurier E 1995 *Phys. Rev.* C **52** R1741
[18] Zuker A P, Poves A, Nowacki F and Lenzi S M 2015 *Phys. Rev.* C **92** 024320
[19] Elliott J P 1958 *Proc. R. Soc.* **245** 128
Elliott J P 1958 *Proc. R. Soc.* **245** 562
[20] Nilsson S G 1955 *Dan. Mat. Fys. Medd.* **29** no. 16
[21] Hara K and Sun Y 1995 *Int. J. Mod. Phys.* E **4** 637
[22] Hara K and Sun Y 1991 *Nucl. Phys.* A **529** 445
[23] Hara K and Sun Y 1991 *Nucl. Phys.* A **531** 221
[24] Hara K and Sun Y 1992 *Nucl. Phys.* A **537** 77
[25] Sun Y and Egido J L 1994 *Nucl. Phys.* A **580** 1
[26] Schmid K W and Grümmer F 1987 *Rep. Prog. Phys.* **50** 731
[27] Schmid K W 2004 *Prog. Part. Nucl. Phys.* **52** 505
[28] Petrovici A, Schmid K W and Faessler A 2000 *Nucl. Phys.* A **665** 333
[29] Brandolini F *et al* 1998 *Nucl. Phys.* A **642** 387
[30] Caurier E *et al* 1995 *Phys. Rev. Lett.* **75** 2466
[31] Hara K, Sun Y and Mizusaki T 1999 *Phys. Rev. Lett.* **83** 1922
[32] Mizusaki T, Otsuka T, Utsuno Y, Honma M and Sebe T 1999 *Phys. Rev.* C **59** R1846
[33] Svensson C *et al* 2000 *Phys. Rev. Lett.* **85** 2693
[34] Svensson C *et al* 2001 *Phys. Rev.* C **63** 061301
[35] Long G L and Sun Y 2001 *Phys. Rev.* C **63** 021305(R)
[36] Caurier E, Nowacki F and Poves A 2005 *Phys. Rev. Lett.* **95** 042502
[37] Kuo T T S and Brown G E 1968 *Nucl. Phys.* A **114** 241
[38] Caurier E, Zuker A P, Poves A and Martinez- Pinedo G 1994 *Phys. Rev.* C **50** 225
[39] Duflo J and Zuker A P 1999 *Phys. Rev.* C **59** R2347
[40] Bengtsson T and Ragnarsson I 1985 *Nucl. Phys.* A **436** 14
[41] Varshalovich D A, Moskalev A N and Khersonskii V K 1988 *Quantum Theory of Angular Momentum* (Singapore: World Scientific)
[42] Peierls R E and Yoccoz J 1957 *Proc. Phys. Soc.* A **70** 381
[43] Hill D L and Wheeler J A 1953 *Phys. Rev.* **89** 1102
Griffin J J and Wheeler J A 1957 *Phys. Rev.* **108** 311
[44] Goeke K, Garcia J and Faessler A 1973 *Nucl. Phys.* A **208** 477
[45] Grümmer F, Goeke K, Allaart K and Faessler A 1974 *Nucl. Phys.* A **225** 443
[46] Wanke C S and Gunye M R 1976 *Phys. Rev.* C **13** 859
[47] Sun Y, Aprahamian A, Zhang J Y and Lee C T 2003 *Phys. Rev.* C **68** 061301 (R)
[48] Kisslinger L S and Sorensen R A 1963 *Rev. Mod. Phys.* **35** 853
[49] Bes D R and Sorensen R A 1969 *Advances in Nuclear Physics* vol 2 (New York: Plenum) p 129
[50] Baranger M and Kumar K 1968 *Nucl. Phys.* A **110** 490
Baranger M and Kumar K 1968 *Nucl. Phys.* A **110** 529
Baranger M and Kumar K 1968 *Nucl. Phys.* A **122** 241
[51] Kishimoto T and Tamura T 1972 *Nucl. Phys.* A **192** 246
[52] Hasegawa M and Kaneko K 1999 *Phys. Rev.* C **59** 1449
[53] Dufour M and Zuker A P 1996 *Phys. Rev.* C **54** 1641
[54] Andersson C G *et al* 1978 *Nucl. Phys.* A **309** 141
[55] Zhang J Y *et al* 1989 *J. Phys. G: Nucl. Part. Phys.* **13** L75
[56] Zhang J Y, Sun Y, Guidry M, Riedinger L L and Lalazissis G A 1998 *Phys. Rev.* C **58** R2663
[57] Möller P *et al* 1995 *At. Data Nucl. Data Tables* **59** 185
[58] Velazquez V, Hirsch J and Sun Y 1998 *Nucl. Phys.* A **643** 39
[59] Chen F Q, Liu Y X, Sun Y, Walker P M and Dracoulis G D 2012 *Phys. Rev.* C **85** 024324
[60] Gao Z C, Sun Y and Chen Y S 2006 *Phys. Rev.* C **74** 054303
[61] Suhonen J and Civitarese O 1998 *Phys. Rep.* **300** 123
[62] Raman S *et al* 1987 *At. Data Nucl. Data Tables* **36** 1
[63] Sun Y and Hara K 1997 *Comp. Phys. Commun.* **104** 245
[64] Allaart K *et al* 1988 *Phys. Rep.* **169** 209
[65] Sun Y, Zhang J Y and Guidry M 1997 *Phys. Rev. Lett.* **78** 2321
[66] Zhang J Y, Sun Y, Riedinger L L and Guidry M 1998 *Phys. Rev.* C **58** 868
[67] Al-Khudair F, Long G L and Sun Y 2009 *Phys. Rev.* C **79** 034320
[68] Zhou Z Y, Liu Y X, Yang Y C, Chen F Q and Sun Y 2014 *Chin. Sci. Bull.* **59** 3853
[69] Sun Y 2006 *AIP Conf. Proc.* **819** 30
[70] Mottelson B R and Valatin J G 1960 *Phys. Rev. Lett.* **5** 511
[71] Stephens F S and Simon R S 1972 *Nucl. Phys.* A **183** 257
[72] Sun Y 2004 *Eur. Phys. J.* A **20** 133
[73] Walker P M and Dracoulis G D 1999 *Nature* **399** 35
[74] Sun Y, Zhou X R, Long G L, Zhao E G and Walker P M 2004 *Phys. Lett.* B **589** 83
[75] Yang Y C, Sun Y, Zhu S J, Guidry M W and Wu C L 2010 *J. Phys. G: Nucl. Part. Phys.* **37** 085110
[76] Herzberg R D and Greenlees 2008 *Prog. Part. Nucl. Phys.* **61** 674
[77] Herzberg R D *et al* 2006 *Nature* **442** 896
[78] Gao Z-C, Horoi M and Chen Y S 2015 *Phys. Rev.* C **92** 064310
[79] Sheikh J A and Hara K 1999 *Phys. Rev. Lett.* **82** 3968
[80] Sun Y, Hara K, Sheikh J A, Hirsch J, Velazquez V and Guidry M 2000 *Phys. Rev.* C **61** 064323
[81] Sheikh J A, Sun Y and Palit R 2001 *Phys. Lett.* B **507** 115
[82] Sun Y, Sheikh J A and Long G L 2002 *Phys. Lett.* B **533** 253
[83] Boutachkov P, Aprahamian A, Sun Y, Sheikh J A and Frauendorf S 2002 *Eur. Phys. J.* A **15** 455
[84] Sheihk J A, Bhat G H, Sun Y, Vakil G B and Palit 2008 *Phys. Rev.* C **77** 034313
[85] Sheikh J A, Bhat G H, Palit R, Naik Z and Sun Y 2009 *Nucl. Phys.* A **824** 58
[86] Sheikh J A, Bhat G H, Sun Y and Palit R 2010 *Phys. Lett.* B **688** 305

[87] Soloviev V G 1990 *Fisika* **22** 19
[88] Sun Y and Wu C L 2003 *Phys. Rev.* C **68** 024315
[89] Sun Y and Wu C L 2008 *Int. J. Mod. Phys. E* **17** 159
[90] Cui J W, Zhou X R, Chen F Q, Sun Y and Wu C L 2012 *Chin. Phys. Lett.* **29** 022101
[91] Cui J W, Zhou X R, Chen F Q, Sun Y and Wu C L 2014 *Phys. Rev.* C **90** 014321
[92] Yannouleas C and Landman U 2007 *Rep. Prog. Phys.* **70** 2067
[93] Tomita N 2004 *Phys. Rev.* B **69** 045110
[94] Jiménez-Hoyos C A, Rodriguez-Guzmán R and Scuseria G E 2013 *J. Chem. Phys.* **139** 204102
[95] Jiménez-Hoyos C A, Rodriguez-Guzmán R and Scuseria G E 2013 *J. Chem. Phys.* **139** 224110
[96] Mizusaki T and Imada M 2004 *Phys. Rev.* B **69** 125110
[97] Tomita N 2009 *Phys. Rev.* B **79** 075113
[98] Fernandez M A and Egido J L 2003 *Phys. Rev.* B **68** 184505
[99] Hubbard J 1963 *Proc. R. Soc.* **276** 238C257
[100] Igawa A 1995 *Int. J. Quantum Chem.* **54** 235
[101] Rodriguez-Guzmán R, Schmid K W, Jiménez-Hoyos C A and Scuseria G E 2012 *Phys. Rev.* B **85** 245130
[102] Rodriguez-Guzmán R, Jiménez-Hoyos C A, Schutski R and Scuseria G E 2013 *Phys. Rev.* B **87** 235129
[103] Balian R and Bezin E 1969 *Nuovo Cimento* B **64** 37
[104] Hara K and Iwasaki S 1979 *Nucl. Phys.* A **332** 61
[105] Hara K and Iwasaki S 1980 *Nucl. Phys.* A **348** 200
[106] Liu Y X *et al* 2011 *Nucl. Phys.* A **858** 11
[107] Robledo L M 2009 *Phys. Rev.* C **79** 021302(R)
[108] Onishi N and Yoshida S 1966 *Nucl. Phys.* **80** 367
[109] Neergard K and Wüst E 1983 *Nucl. Phys.* A **402** 311
[110] Robledo L M 2011 *Phys. Rev.* C **84** 014307
[111] Bertsch G F and Robledo L M 2012 *Phys. Rev. Lett.* **108** 042505
[112] Avez B and Bender M 2012 *Phys. Rev.* C **85** 034325
[113] Oi M and Mizusaki T 2012 *Phys. Lett.* B **707** 305
[114] Mizusaki T and Oi M 2012 *Phys. Lett.* B **715** 219
[115] Hu Q L, Gao Z C and Chen Y S 2014 *Phys. Lett.* B **734** 162
[116] Mizusaki T, Oi M, Chen F Q and Sun Y 2013 *Phys. Lett.* B **725** 175
[117] Wang L J, Chen F Q, Mizusaki T, Oi M and Sun Y 2014 *Phys. Rev.* C **90** 011303
[118] Anguiano M, Egido J L and Robledo L M 2001 *Nucl. Phys.* A **696** 467
[119] Dobaczewski J, Stoitsov M V, Nazarewicz W and Reinhard P-G 2007 *Phys. Rev.* C **76** 054315
[120] Lacroix D, Duguet T and Bender M 2009 *Phys. Rev.* C **79** 044318
[121] Duguet T, Bender M, Bennaceur K, Lacroix D and Lesinski T 2009 *Phys. Rev.* C **79** 044320
[122] Poves A and Zuker A 1981 *Phys. Rep.* **70** 235
[123] Otsuka T, Fujimoto R, Utsuno Y, Brown B A, Honma M and Mizusaki T 2001 *Phys. Rev. Lett.* **87** 082502
[124] Otsuka T, Suzuki T, Fujimoto R, Grawe H and Akaishi Y 2005 *Phys. Rev. Lett.* **95** 232502
[125] Otsuka T, Suzuki T, Honma M, Utsuno Y, Tsunoda N, Tsukiyama K and Hjorth-Jensen M 2010 *Phys. Rev. Lett.* **104** 012501
[126] Kaneko K, Mizusaki T, Sun Y and Tazaki S 2014 *Phys. Rev.* C **89** 011302(R)
[127] Kaneko K, Mizusaki T, Sun Y and Tazaki S 2015 *Phys. Rev.* C **92** 044331